Rusydy *et al. Geoenvironmental Disasters* (2024) 11:28
https://doi.org/10.1186/s40677-024-00290-9

Geoenvironmental Disasters

REVIEW Open Access

The development and implementation of design flowchart for probabilistic rock slope stability assessments: a review

Ibnu Rusydy[1,2], Ismet Canbulat[1], Chengguo Zhang[1*], Chunchen Wei[1] and Alison McQuillan[3]

Abstract

Background Rock slope instability is a complex geotechnical issue that is affected by site-specific rock properties, geological structures, groundwater, and earthquake load conditions. Numerous studies acknowledge these aleatory uncertainties in slope stability assessment; however, understanding the rock behaviour could still be improved. Therefore, this paper aims to summarise the probability methods applied in rock slope stability analysis in mining and civil engineering and develop new probabilistic design and assessment methodologies for four methods, namely empirical/rock mass classifications techniques, kinematic analysis, limit equilibrium (*LE*), and numerical methods and introduces how to integrate all methods to determine the total probability of failure. The case studies have been conducted based on slopes from Indonesia, a seismically active country, utilising the proposed design methods.

Results Regarding the probabilistic empirical/rock mass classification (RMC) technique, this study has identified that seven of the ten most involved input parameters in RMC naturally exhibit aleatory uncertainty. Thus, the optimal way to present the output probability of RMC is as a confidence interval (*CI*) or total and conditional probability associated with each rock mass class. In probabilistic kinematic analysis, this study presents a systematic method to compute the probabilities of different types of failure alongside the total probability of occurrence (P_{tK}). The probability of failure (*PoF)* for jointed generalized Hoek-Brown (GHB) numerical modelling was lower than that obtained through the probabilistic *LE* approach for a similar slope. However, the *PoF* of jointed GHB is higher than the *LE* approach when loaded with 0.1 and 0.15 earthquake coefficients.

Conclusions The variation of *PoF* across different failure criteria determines how epistemic uncertainty is apparent in the modelling process, while the aleatory uncertainty arises from input parameters. Furthermore, this study introduces the total probability of failure equation as a combination of kinematic and kinetic probabilities (limit equilibrium and numerical modelling).

Keywords Probabilistic, Rock slope, Slope stability, Probability of failure

*Correspondence:
Chengguo Zhang
chengguo.zhang@unsw.edu.au
[1]School of Minerals and Energy Resources Engineering, Engineering Faculty, UNSW, Sydney 2052, Australia
[2]Department of Geological Engineering Department, Engineering Faculty, Universitas Syiah Kuala, Aceh 23111, Indonesia
[3]Rocscience Inc., Gold Coast, Australia

Introduction

Maintaining rock slope stability is the primary objective of any open cut/pit slopes. However, achieving a completely stable slope may be challenging due to the inherent nature of the heterogeneous properties of rock mass (Abdulai and Sharifzadeh 2019, 2021; Aladejare and Akeju 2020; Asem and Gardoni 2021; Basahel and Mitri 2019; Huang et al. 2023; Obregon and Mitri 2019; Rusydy et al. 2022). The variability of rock properties leads to uncertainty in determining the input values for rock slope stability analyses, directly impacting its output and safe slope design. The variability is defined as the multiple values of the quantity of the rock properties at different points and times (Begg et al. 2014; Hsu and Nelson 2006; Zhang Wg et al. 2021). Other researchers define variability as the total unpredictability value of the system or parameters (Bedi 2013). The variability can be quantified by the frequency distribution of the collected data, whilst the probability distribution quantifies the uncertainty leading by variability (Bedi 2013; Begg et al. 2014). Thus, the probability analysis can help address the uncertainties in rock slope stability analysis.

Numerous studies recently acknowledged the aleatory and epistemic uncertainties in their analysis of rock slope stability analysis. The aleatory uncertainty arises due to geological processes which are inherent in rock. The epistemic uncertainty is mostly due to a lack of knowledge, input data or measurement error (Abdulai and Sharifzadeh 2019; Baecher and Christian 2005; Lu et al. 2019).Both uncertainties often occur in rock slope stability analysis. how to overcome those uncertainties for four rock slope stability methods are unwell explain inform of exhaustive designs flowchart in previous studies. Furthermore, Budetta (2020); Obregon and Mitri (2019) emphasised that combining rock slope stability methods will yield reliable results. This review comprehensively explains the methodology to integrate all methods in the probability approach.

This study aims to review the probability methods applied in rock slope stability analysis and develop a new design and assessment flowchart for probability analysis employing empirical/rock mass classifications, kinematic analysis, limit equilibrium (*LE*), and numerical methods. Furthermore, this paper provides case studies using the proposed flowcharts to analyse the probability of rock slope failures using those four methods. Lastly, this study introduces the total probability of failure by integrating all probability results.

Rock slope in civil and mining engineering projects

Numerous civil engineering and mining projects focus on rock mass and cutting rock slope. Both civil and mining projects have specific performance criteria regarding slope design, reliability, and stability approaches. Several distinct performance requirements between the two projects are related to the degree of reliability, degree of normal stress, degree of asperities or joint roughness, degree of stand-up time for long-term stability, degree of geology structures involvement, and the factor of safety (*FoS*). Figure 1 illustrates the differences between civil and mining engineering projects in a spider chart.

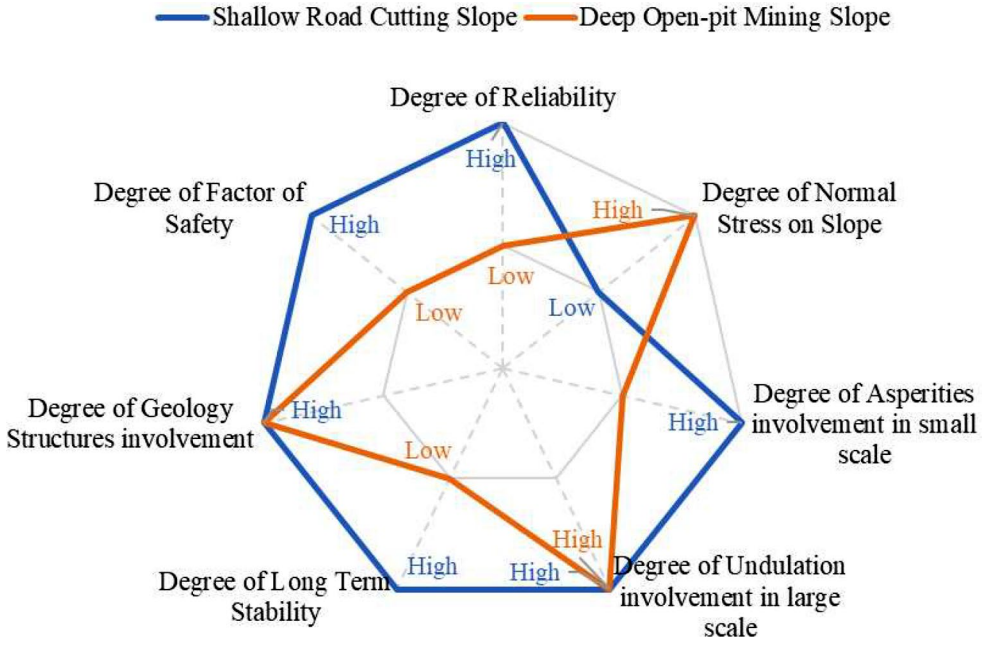

Fig. 1 Difference between road-cutting rock slopes and open-pit mining rock slopes

Civil engineering projects have a high demand for reliability and safety compared to the rock slope for open-pit mining (Wyllie 2018; Wyllie and Mah 2004). For instance, the slope height in open-pit mining is higher, and the slope is designed for 5 to 50 years of operation. In civil engineering projects (e.g., road-cutting rock slopes), the height of slopes is relatively low, but it is common to design them to last over 100 years (Basahel and Mitri 2019). In mining projects, slope usually can be accommodated, provided that failure is not a "surprise". On the other hand, the slopes in civil engineering should not fail due to the risk to the public. In both projects, several combinations of slope angles are chosen based on the rock mass quality and geological structure orientation.

Furthermore, the road-cutting rock slopes are designed in a high-reliability state. A small failure on the slope will lead to transportation interruption, risk to the public, and an economic impact. Hence, the *FoS* of rock slopes in civil engineering projects is significantly higher than in open-pit mining slopes. Basahel and Mitri (2019) state that the *FoS* in civil engineering projects is approximately 1.5. In addition, the design of the road-cutting rock slope in civil engineering projects focuses more on the geological structure than the stresses acting on the slope due to the shallow depths (Keneti et al. 2021; Wyllie 2018; Wyllie and Mah 2004). In shallow slopes, where the normal stress is the low or de-stressed area, the geological structures tend to influence rock slope stability more than most critical factors. Thus, Barton (2013) and Li et al. (2020) note that it is unlikely for intact rock to fracture at a low normal stress environment where the dilation stress is dominant in shear behaviour. In large open pits, the normal/gravitational stress controls the stability of the slope (Stead and Wolter 2015).

In high normal-stress slopes, a small scale of roughness no longer affects the shear strength of the rock slope and can be neglected. Nevertheless, according to Barton and Bandis (1982), the large scale of undulation in the discontinuity plane still plays a significant role under relatively high normal stress conditions. In addition, open-pit mining still considers the geological structures to assess the slope stability. The other four categories, such as degree reliability, probability of failure (*PoF*), degree of asperities, and long-term stability, are less concerned in mining projects. This phenomenon occurs due to short-term mining operations. Neither civil nor mining projects cannot neglect the geological structure uncertainty which is inherent in rock (aleatory uncertainty) when studying rock slope stability. Geological structures play an important role in nature and engineered rock slopes, determining the failure typologies, mechanism, failure initiation, and style (Stead and Wolter 2015). The failure typologies are driven by the orientation of geological structures or discontinuity planes (Barton 1973; Rusydy et al. 2019, 2021, 2022). While the failure mechanism is influenced by the composition and geometry of rock slope (Stead and Wolter 2015). Furthermore, the discontinuity planes decrease the strength and stiffness of rock mass (Zhao et al. 2023).

Assessment methods for rock slope stability

The rock slope stability methods are divided into four main approaches: empirical, kinematical, limit equilibrium, and numerical modelling. In rock engineering, empirical and kinematic analyses are employed in rock slope design without incorporating the *FoS*. While the limit equilibrium and numerical modelling can compute the *FoS* and assess the critical failure mechanism (Abdulai and Sharifzadeh 2019; Hussain et al. 2021; Sari 2019). Sari (2019) emphasises that all those methods had to be conducted to reach reliable and satisfactory rock slope stability analysis and design. However, McQuillan et al. (2020) note that limit equilibrium modelling and kinematic analysis are the most routine methods applied in the coal mining industry, followed by empirical and numerical modelling, especially in Australia. This section will provide a systematic explanation of four rock slope stability assessments.

Empirical rock mass classification approaches

The empirical rock mass classifications provide the basic knowledge of empirical design in rock engineering. The rock mass classification system fosters communication between geologists, contractors, mining engineers, and civil engineers (Cai 2011; Rusydy and Al-Huda 2021; Zhang et al. 2019). The empirical and classification approaches in rock support design are the most practical, assuming that investigated rock masses are identical to the previous case studies (Cai 2011). To date, a multitude of rock mass classifications have been developed in rock mechanics. The most widely employed methods are the rock mass rating (RMR89) of Bieniawski (1989), the Q-system developed by Barton et al. (1974), and the Geological Strength Index (GSI) introduced by Hoek and Brown (1997). For rock slope stability design, the engineers employ Slope Mass Rating (SMR) from Romana (1985), which is a modified version of RMR89 by adding the adjustment factors (*F1*, *F2*, *F3*, and *F4*). In addition, many new classification techniques have been introduced in recent years.

The development of rock mass classifications for different applications from 1946 to the present is denoted in Fig. 2a. In the first era of development, most classifications were developed for tunnel design, followed by general purposes (tunnelling and cutting) that were initiated in 1973 when Bieniawski initiated his first RMR73 and updated to RMR89. The latest modifications of the RMR89 have been made by Celada et al. (2014) for

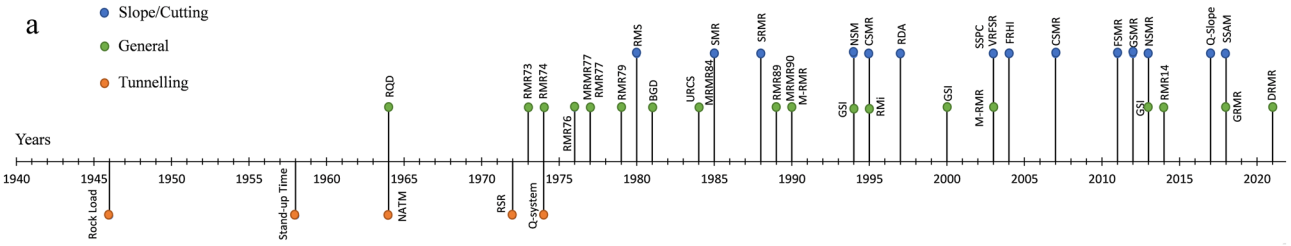

b

Rock Classifications and Involved Parameters	RMR_{89}	RMS	SMR	SRMR	GSI_{95}	CSMR	GSI_{2000}	RDA	SSPC	VRFSR	FRHI	Q-Slope	SSAM	NSMR	Total Involved (n)	Score (Sc) = n/N	Weigth = Sc/T_{Sc} x 100
	Total of Rock Mass Classifications (N) = 14																
Spacing	✓	✓	✓	✓	✓	✓		✓	✓	✓	✓			✓	11	0.79	13
Joint Condition & Aperture	✓		✓	✓	✓	✓	✓		✓	✓		✓	✓	✓	11	0.79	13
Intact Rock Strength	✓	✓	✓	✓	✓	✓		✓	✓	✓				✓	10	0.71	11
RQD	✓		✓	✓	✓	✓		✓	✓	✓		✓		✓	10	0.71	11
Groundwater	✓	✓	✓			✓	✓	✓		✓			✓	✓	9	0.64	10
Orientation of Joint	✓	✓	✓			✓			✓	✓		✓	✓	✓	9	0.64	10
Disintegration of Rock Mass		✓					✓	✓	✓		✓	✓	✓	✓	8	0.57	9
Slope Angle			✓			✓			✓	✓	✓		✓	✓	7	0.50	8
Excavation Methods			✓			✓		✓	✓	✓	✓			✓	7	0.50	8
Slope Height						✓		✓	✓	✓	✓		✓		6	0.43	7
															Total Score (T_{Sc})	6.29	

c

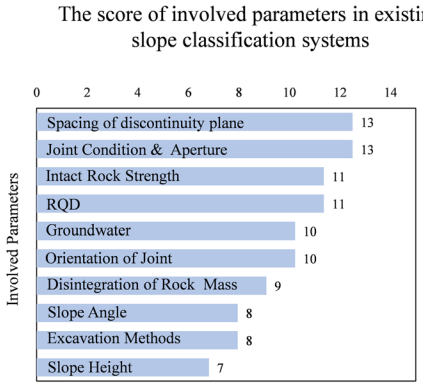

Fig. 2 (**a**) The history of rock mass classifications timeline, (**b**) and (**c**) are the resumes of the involved parameters in slope classification systems. Some data are retrieved from Pantelidis (2009), Zheng et al. (2016), and literature studies

RMR14, Maazallahi and Majdi (2021) for DRMR, and Azarafza et al. (2022) for soft rock slope design. Furthermore, the classification for rock slope analysis was initiated by Selby (1982), who developed rock mass strength (RMS). Recently, Bar and Barton (2017) proposed the Q-slope, a modification approach from the previous Q-system of Barton et al. (1974). McQuillan et al. (2018) developed the Slope Stability Assessment Methodology (SSAM) in a mining project, employing ten important parameters in rock slope stability analysis and design.

Regarding the important parameters critical in slope stability, Pantelidis (2009) recognises the top ten parameters employed in rock mass classifications for rock cut slopes. These parameters are intact rock strength, rock quality designation (*RQD*), spacing, joint condition, groundwater, slope height, slope angle, degree of weathering, method of excavation/cutting, and joint orientation. This review has computed the weight of each parameter based on 11 classification techniques from Pantelidis (2009).The three latest additional classifications are Q-slope (2017), SSAM (2018), and NSMR (2013) from our analysis as denoted in Fig. 2b. All 14 classification techniques (*N*) are utilised to determine the weighting of each parameter, as shown in Fig. 2c. The scoring analysis indicates that the top five parameters significantly involved in slope analysis are spacing of discontinuity planes, joint condition and aperture, strength of intact rock, RQD, and groundwater. Those parameters are essential for slope stability analysis in empirical rock mass classification approaches.

Numerous researchers conducted probabilistic rock mass classification. Sari et al. (2010) performed a Monte Carlo Simulation (MCS) to determine the RMR and GSI classifications for 3 types of Ankara andesite. On the other hand, Cai (2011) employed MCS to determine the input variable for GSI, whilst Bedi (2013); Lu et al. (2019) employed MCS to analyse the input variable for Q-system in tunnelling design.

Kinematic analysis approach

The rock slope kinematic approach can determine the typology of slope failure from geometry evaluation of dips (β_j), dip directions (α_j), slope angle (β_s), slope direction/face/aspect (α_s), and friction angle (Φ). Barton (1973) emphasised that the orientation of discontinuity planes will determine the mode of failures in rock slopes. In the conventional deterministic approach, the single mean values of dip and dip directions from the stereography projection techniques are utilised to determine the type of failure, as shown in Fig. 3a. Basahel and Mitri (2019) emphasise that the discontinuity planes in rock mass are considered the source of uncertainty in the analysis.

Numerous researchers have conducted probabilistic kinematic analyses in recent years. Park et al. (2016) conducted a probabilistic kinematic analysis using a GIS-based approach. The probabilistic kinematic conducted

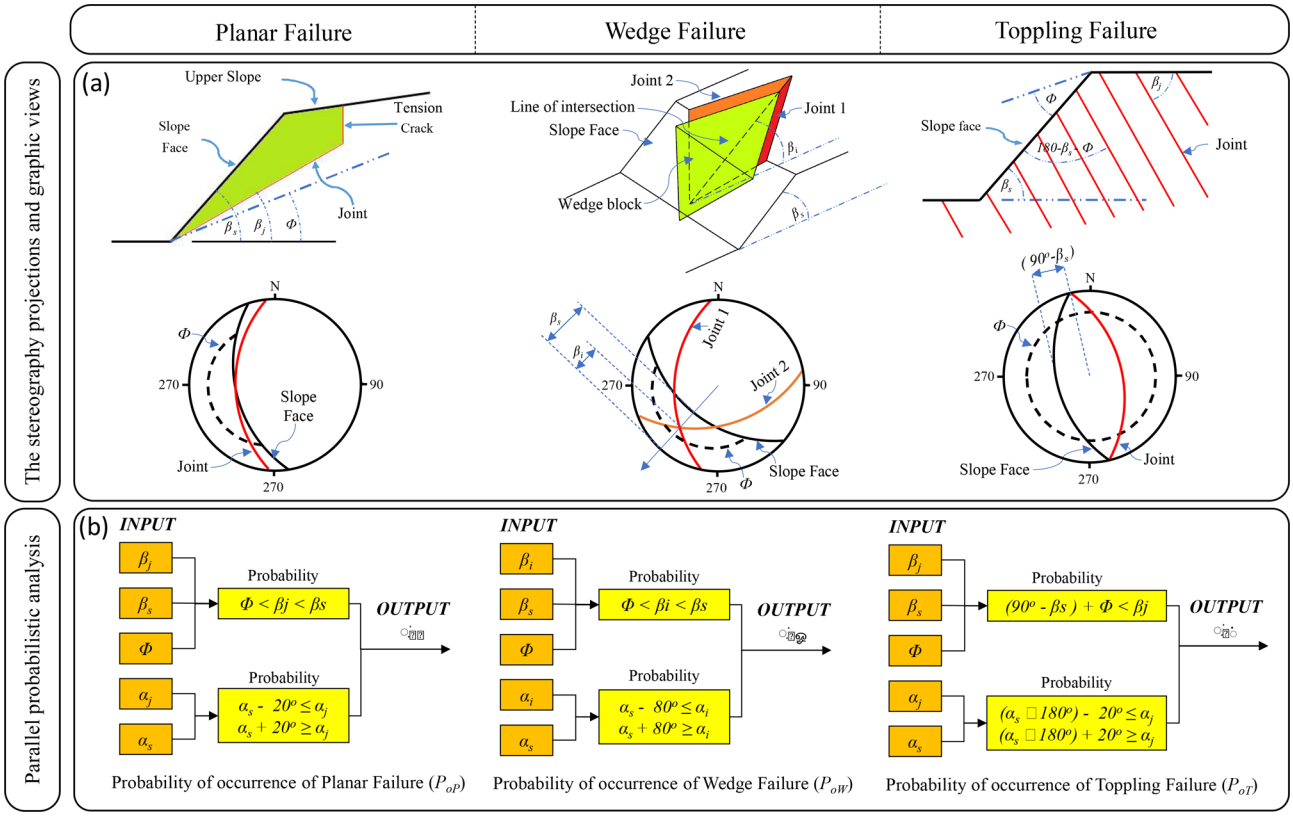

Fig. 3 (**a**) The graphic and stereography projections for three types of rock failures (modified from Wyllie and Mah (2004), (**b**) the parallel systems for calculating the probability of occurrence refers to Rusydy et al. (2022) and Obregon and Mitri (2019)

by Park et al. (2016) was a stochastic approach generating 20,000 random values of Monte Carlo simulation based on statistical properties of the input variables (β_j, α_j, β_s, α_s). On the other hand, Zhou et al. (2017) and Yan et al. (2022) employed the Bayesian approach in their probability analyses.

The probabilistic analysis acts in two systems: a series and parallel system (Obregon and Mitri 2019; Park and West 2001; Zhao et al. 2016), and those systems are reasonably reliable to be implemented in probabilistic kinematic analysis (Fig. 3b). In the series system, when one parameter fails, it will lead to the failure of the entire system, such as rock slope failure. On the other hand, in a parallel system, the rock slope failure will only occur when all parameters fail. Hence, all conditions are required for the slope to fail.

The kinematic analysis requires numerous geometrical conditions for the slope to fail. For instance, the planar failure will occur in conditions where the dip of the discontinuity plane (β_j) is higher than the friction angle (Φ) but lower than the slope angle (β_s). Another condition is that the dip direction (α_j) must be within 20° of the slope face (α_s) (Wyllie 2018; Wyllie and Mah 2004). This planar failure condition is expressed in Eq. 1. The other requirements for wedge and toppling failures are defined in Eqs. 2 and 3, respectively, as Obregon and Mitri (2019) suggest for the parallel system.

$$P_{oP} = \Pr[\phi \le \beta_j \le \beta_s] \cdot \Pr[\alpha_s - 20^\circ \le \alpha_j \le \alpha_s + 20^\circ] \quad (1)$$

$$P_{oW} = \Pr[\phi \le \beta_i \le \beta_s] \cdot \Pr[\alpha_s - 80^\circ \le \alpha_i \le \alpha_s + 80^\circ] \quad (2)$$

$$P_{oT} = \Pr[(90^\circ - \beta_s) + \phi \le \beta_j] \cdot \Pr[(\alpha_s \pm 180^\circ) - 20^\circ \le \alpha_j \le (\alpha_s + 180^\circ) + 20^\circ] \quad (3)$$

Limit equilibrium approach

Rock slope stability relies on the shear strength (τ) of discontinuity planes and rock mass developing on the slip zone of the rock slope. In planar failure, the rock material can be assumed to be Mohr-Coulomb (MC) material, in which the shear strength is expressed in cohesion (c) and friction angle (Φ) in a linear pattern (Wyllie and Mah 2004). Barton (2013) emphasises that the shear strength of intact rock, non-planar rock joints, and rockfill are determined as non-linear shear strength patterns. The rock slope failure can occur either along the discontinuity

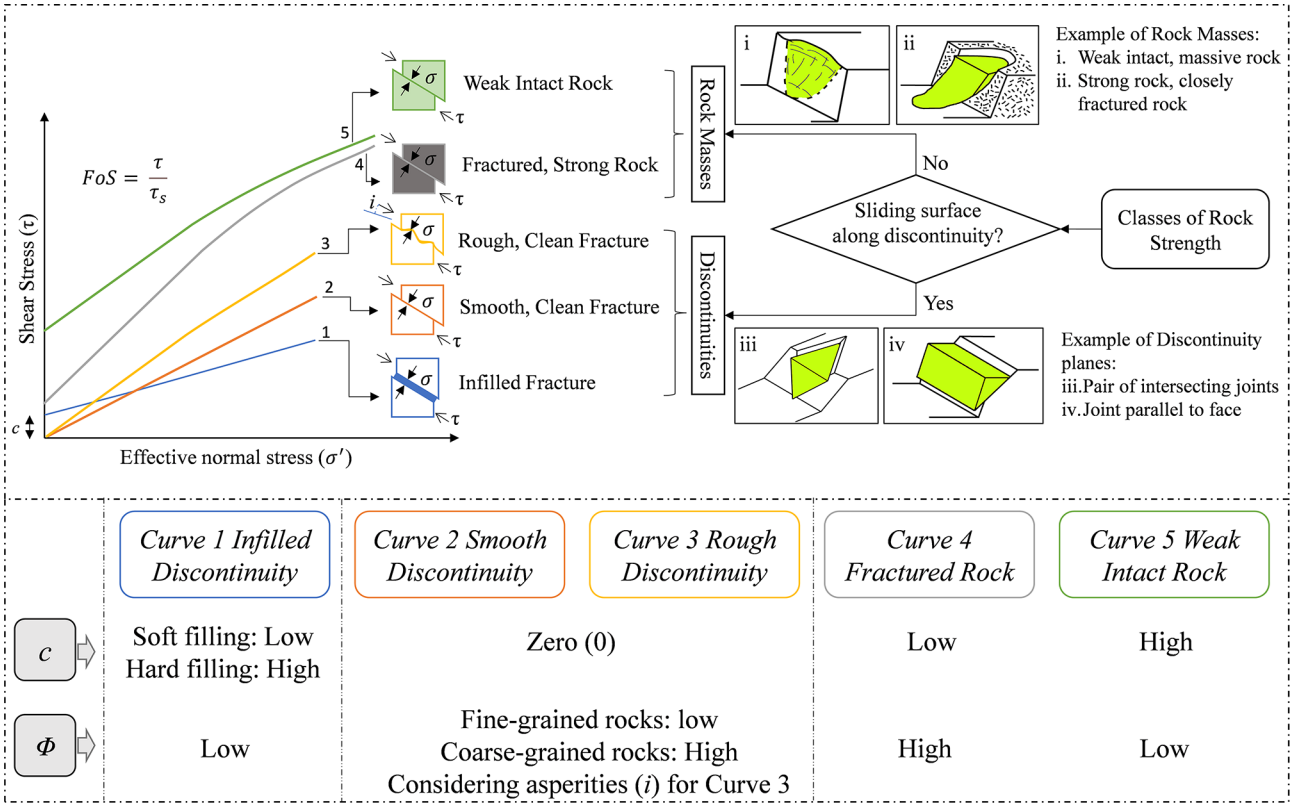

Fig. 4 (**a**) The Five geological conditions and their relationship stresses (normal and shear) on Mohr diagram and rock shear strength classes after modified from Wyllie and Mah (2004), (**b**) cohesion (**c**) and friction angle (Φ) in different types of geological conditions

planes or along the weak zone in the rock mass. Hence, Wyllie and Mah (2004) classify rock shear strength into the shear strength of discontinuities and the shear strength of rock masses, as illustrated in Fig. 4a.

The shear strength of discontinuities is influenced by friction angle and irregularity of discontinuity planes, namely asperities (*i*), as defined by Patton (1966). These asperities influence the discontinuity shear strength, especially in low normal-stress rock slopes. According to Barton (1973), the asperities can be computed from surface joint roughness coefficient (*JRC*), joint compressive strength (*JCS*), and effective normal stress (σ'). When discontinuity planes are filled with soft materials (curve 1 in Fig. 4a), the shear strength is commonly lower than the clean discontinuity plane (Pereira 1997). This condition occurs because the infilled material controls the shear strength, not the joints' shear strength. When the discontinuity plane is filled with weak clay, cohesion is clay's cohesion. In contrast, if the cohesion of the discontinuity planes is clean (see curves 2 and 3 in Fig. 4), the cohesion is zero ($c=0$), but the friction angle depends on roughness of the surface plane and ratio between normal stress and rock strength (Barton 2013; Wyllie and Mah 2004).

Regarding the shear strength of rock masses, the failure in rock masses is a combination of failure in sliding surfaces with the failure of intact rock between discontinuity planes. Thus, the shear strength of rock masses is defined as the shear strength of intact rock bridges combined with the shear strength on the discontinuity planes at larger strain (Barton 2013; Barton and Pandey 2011). The rock mass and intact rock act as isotropic behaviour. The shear strength can be calculated by employing either Mohr-Coulomb (MC) or Hoek-Brown (HB) failure criteria (Sari 2019), or Barton-Bandis (BB) criteria as suggested by Barton (2013). As shown in Fig. 4a, the rock mass failure occurs in heavily fractured rock masses and weak massive rock. Sari (2019) emphasises that the HB was primarily developed for homogeneous rock mass with a non-sliding failure plane. Furthermore, the shear strength behaviour determines the *FoS* of the rock slope. The *FoS* commonly used in mining projects is 1.2 to 1.4 (Wyllie and Mah 2004); nevertheless, the *FoS* of rock slope in civil engineering projects is commonly 1.5 (Basahel and Mitri 2019).

The *FoS* is the ratio of shear strength (resisting forces) to the shear stress (driving forces) acting on the slope. In the deterministic approach, the *FoS* is calculated by assigning a single value to each parameter and neglecting the variability of input parameters. To quantify this challenge, the PoF has been introduced in probabilistic limit equilibrium analysis for mining and civil engineering projects. The *PoF* is computed using a similar procedure

to FoS, examining the shear strength (resisting forces) and the shear stress (driving forces) acting on the slope using the appropriate input parameter distribution and the stochastic modelling approach. In other words, the *PoF* defines the probability of $FoS < 1.0$ or reference values from the simulations (Abdulai and Sharifzadeh 2021; Aladejare and Akeju 2020; Obregon and Mitri 2019). The margin of safety determines the difference between resisting forces and driving forces. Hence, the negative value of the margin of safety demonstrates an unstable rock slope.

Numerical modelling approach

The numerical modelling method is an improvement from the limit equilibrium method, which is limited in calculating the *FoS.* The limit equilibrium method assumes the slope materials have rigid behaviour, and all the forces act in virtue of the centre of gravity. Numerical modelling such as finite element method (FEM), finite difference method (FDM), boundary element method (BEM), distinct element method (DEM), and hybrid methods are rigorous methods to understand the displacement direction or deformation and stress analysis in geomechanics (Zhang et al. 2012). The computer program of numerical modelling seeks to determine the initial condition of rock mass mechanical response from in situ stress, boundary conditions, etc. The rock slope materials are subdivided into small zones, each with specific rock material properties assigned. Those material models are assumed ideally to be a stress/strain relationship. When these zones are linked, it is named a continuum model, but when they are not connected and separated by discontinuity planes, it is referred to as a discontinuum model (Wyllie and Mah 2004).

A different approach to computing the *FoS* is applied in numerical modelling with a finite element program where the shear strength is reduced before the slope fails (Hammah et al. 2009; Shen 2012; Wyllie 2018). This technique is known as the Shear Strength Reduction Method (SRM). Zienkiewicz et al. (1975) introduced the SRM during the early period of finite element modelling when they studied the stability and deformation of embankment slopes by reducing shear strength properties. Recently, this method has been implemented by many other authors to determine the *FoS* in mining and civil engineering projects (Abdulai and Sharifzadeh 2019, 2021; Basahel and Mitri 2019; Brideau et al. 2012; Hammah et al. 2009; Hussain et al. 2021; Sari 2019; Shen 2012; Stead et al. 2006).

According to Wyllie (2018), the SRM approach has two primary improvements compared to the limit equilibrium method; the sliding plane and satisfy equilibrium for a different type of failure are determined automatically. In addition, numerical modelling can model the continuum and discontinuum of rock mass behaviour unaccompanied by prior assumptions (Hammah et al. 2009). The limit equilibrium method cannot fulfil all those advantages in numerical analysis. Numerical modelling can also explicitly calculate the stress and displacements of the rock mass, considering site-specific conditions. The example output of numerical modellings for rock slope stability analysis are illustrated in Fig. 5.

Numerical modelling is an advanced approach to rock slope stability analysis. Nevertheless, each method has its advantages, disadvantages, range of applicability, and

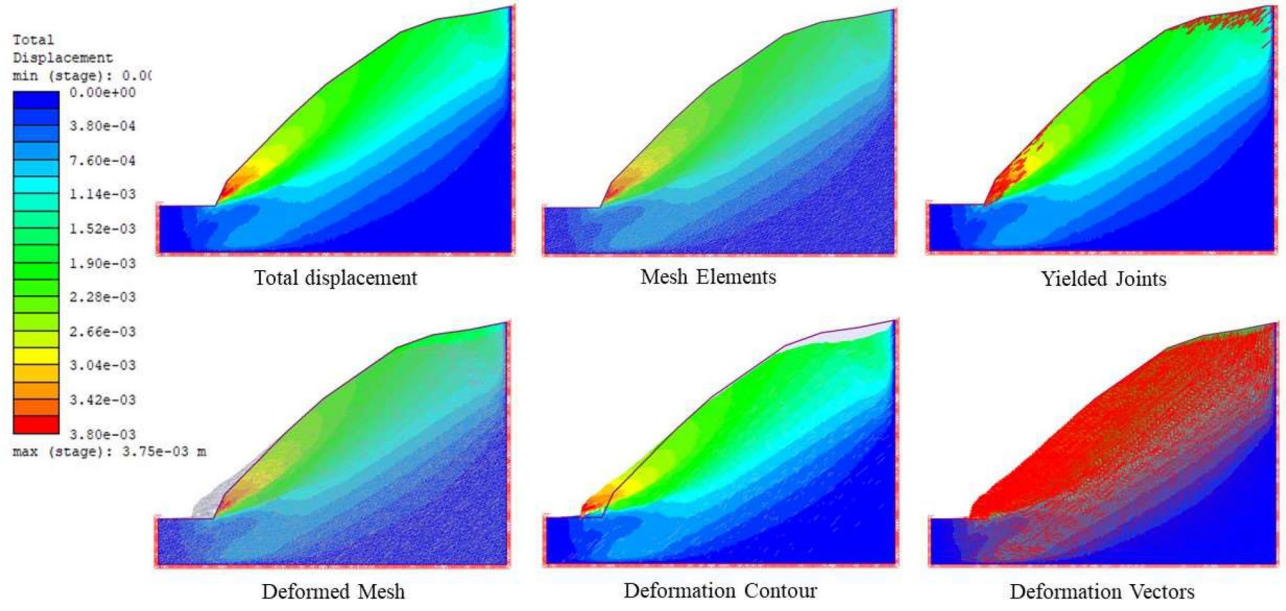

Fig. 5 The example of numerical modelling using FEM for rock slope stability and its outputs

Table 1 The comparison between the slope stability assessment methods

Aspects	Numerical Modelling	Limit Equilibrium method	Rock Kinematic Analysis	Empirical and Classification Method
Advantages	- Displacement direction or slope deformation. - Yields the *FoS*. - Does not require a failure plane. - Non-rigid material behaviour.	- Yields the *FoS*. - Able to calculate manually.	- Able to calculate manually. - Yields the type of failure.	- Provide basic knowledge of rock quality. - Able to calculate manually. - Rock mass quality in quantitative approach
Disadvantages	- Require high-performance computer for large-scale model	- Require failure plane. - Rigid material behaviour. - Forces acting at the centre of gravity.	- Ignore the force working the slope. - Unable to determine Factor of Safety *FoS*.	- Unable to determine Factor of Safety *FoS*.
Applicable Range as Regard Geological Conditions (Refer to Fig. 4)	- Infilled fracture - Smooth and clean fracture - Rough and clean fracture - Fractured and strong rock - Weak intact rock	- Infilled fracture - Smooth and clean fracture - Rough and clean fracture - Fractured and strong rock	- Smooth and clean fracture - Rough and clean fracture	- Infilled fracture - Smooth and clean fracture - Rough and clean fracture - Fractured and strong rock
Deterministic Output	Slope Deformation, stress, and *FoS*	*FoS*	Type of Failure	Quantitative value and rock mass classes
Probabilistic Output	*PoF* and Reliability Index (*RI*)	The *PoF* and Reliability Index (*RI*)	The total probability of occurrence (*PtK*)	The conditional probability of each class

output, as shown in Table 1. Considering all discontinuity planes in numerical models is challenging, particularly for extensive isotropic or anisotropic rock slopes. When the numerical model uses the HB criteria, the GSI must be between 30 and 80, as the HB failure criterion is inapplicable for very hard rock/brittle response (GSI > 80) and soft rocks (GSI < 30) (Wyllie 2018).

Most numerical modelling in rock slope assessments employs the HB failure criterion rather than the MC failure criterion. Furthermore, Barton (2013) emphasised that the HB with a non-linear strength criterion is more reliable in rock shear analysis than MC having a linear strength pattern. Moreover, Hussain et al. (2021) compared the *FoS* under both failure criteria; revealing that the MC method tends to yield higher values of *FoS* compare to HB. Barton (2013) noted that the failure in the rock mass is due to the failure in the rock intact bridge combined with the failure along a discontinuity plane. Different scales of rock mass yield distinct shear strength. Accordingly, scale-effect correction must be performed using Barton and Bandis (1982) law for jointed rock mass. Scale-effect is also related to the block size effect on jointed rock. According to Barton and Bandis (1982), shear strength and stiffness will eventually decrease as the block size increases due to a reduction of effective joint roughness.

As mentioned previously, numerical modelling encompasses various methods, including FEM, FDM, BEM, DEM, and hybrid methods. Each method has advantages and disadvantages. According to Zhang et al. (2012), FEM has limitations related to the mesh size effect; FDM struggles with regular grid systems when it includes fracture integration and inhomogeneity of material. However, both FEM and FDM can deal with non-linearity material within the model. The BEM has limitations in simulating the inhomogeneous and non-linear materials. In contrast, DEM can work with inhomogeneous material and incorporates the discontinuity planes into the model (Zhang et al. 2012). In summary, FEM, FDM, and BEM are typically utilised to simulate continuum models, while DEM is used for discontinuum models in rock slope stability analysis.

The probabilistic approaches in rock slope stability

The probabilistic approach is an advanced method compared to the deterministic. A single mean value is utilised in deterministic as an input parameter to produce a single output value (Abdulai and Sharifzadeh 2019, 2021; Basahel and Mitri 2019; Obregon and Mitri 2019). The probabilistic approaches have been prevalent in the recent decade (Ahmadabadi and Poisel 2016). The following paragraphs elaborate on three popular probabilistic slope stability approaches.

The Monte Carlo Simulation (MCS) is the most frequently used method in stochastic analysis in generating random values of rock properties employing Simple Random Sampling (SRS) or Latin Hypercube Sampling (LHS). Hammah et al. (2009) note that MCS can generate multiple output responses in one model, which is qualified to deal with multiple types of probability distributions and develop a model correlation between variables. In multiple variables, Millard (2013) emphasises that if all variables have an identical data distribution, it can directly generate the correlated random number. However, if each variable has its distribution, it must employ rank correlations.

The second method is the Point Estimate Method (PEM), introduced by Rosenblueth (1981) to develop a

Table 2 Frequentist versus bayesian statistic in rock engineering

No.	Condition and Aspect	Frequentist	Bayesian
1.	Observed data	As random values	As random values
2.	Observed data properties (e.g., μ, σ)	As fixed value	As random values
3.	Prior data distributions	Not considered	Considered
4.	Terminology of 95% boundaries	Confidence intervals (*CI*): uncertainty in the interval	Credible intervals (*CI*): uncertainty in the parameter. High-density interval (HDI)
5.	Interpretation	Rely on sample information	Rely on prior and sample information
6.	Probability as the degree of belief	Considered	Considered
7.	Result interpretations	Maximum likelihood, *CI*, and null hypothesis	Updating knowledge (posterior) based on prior and sample information.

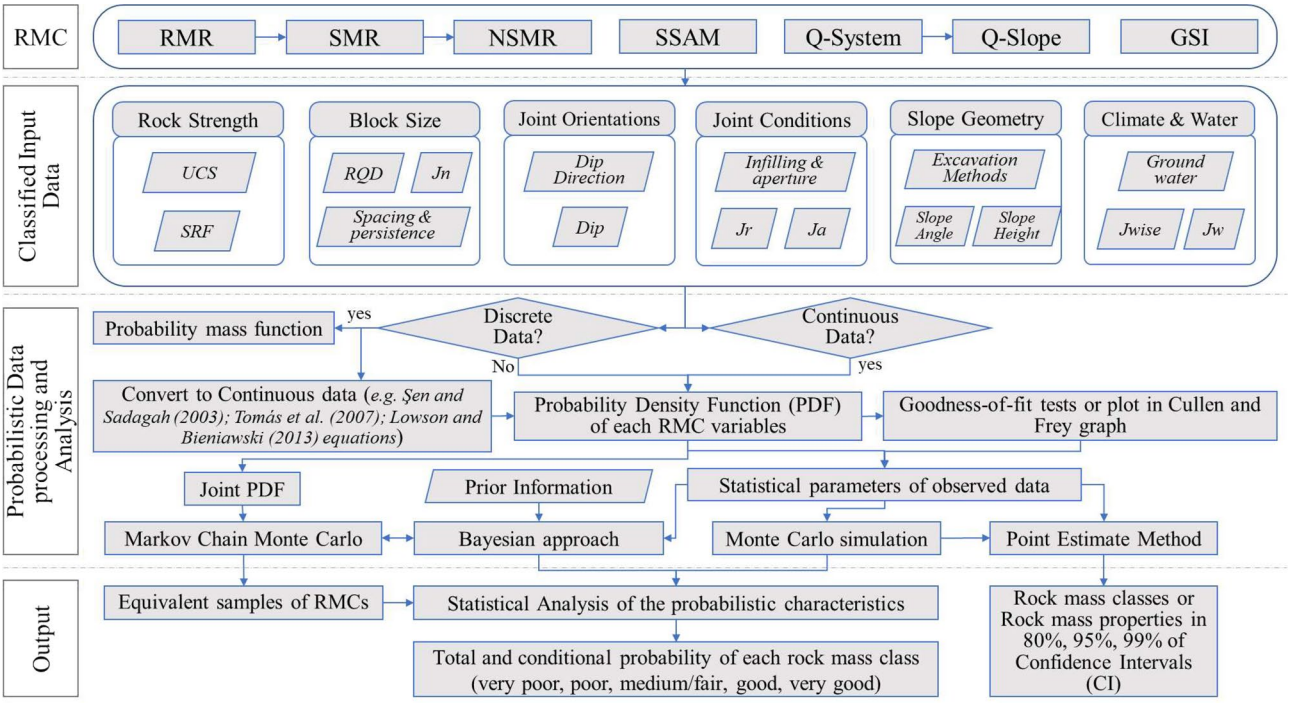

Fig. 6 The proposed flowchart for probabilistic analysis of rock mass classifications (RMCs)

straightforward method to estimate statistical moments such as the standard deviation, mean, and skewness. A comprehensive study regarding PEM for probabilistic analysis in rock slope was conducted by Ahmadabadi and Poisel (2016), dealing with non-normal data distribution typology employing four types of PEMs: Rosenblueth's PEM, Zhou and Nowak's PEM, Harr's PEM, and Hong's PEM. The result of the PEM approach is reliable and accurate in numerous conditions regardless of its simplicity compared to MCS, requiring a high number of simulations. This compassion has been conducted by Hammah et al. (2009) and Park et al. (2012).

The third method is Bayesian statistics. Different from frequentist statistics treating the observed data as random variables while its statistical parameters (e.g., mean, standard deviation) are a single unknown value, the Bayesian statistic considers both observed data and statistical parameters as random variables (Contreras et al. 2018; Feng et al. 2020). The Bayesian approach starts by determining the likelihood function before deciding the parameter of the prior distribution to compute the posterior distribution (Feng et al. 2020).

As for rock engineering study, the Bayesian approach has been adopted by numerous researchers to quantify the uncertainty in rock strength, stresses, and other rock properties for intact rock and rock mass (Aladejare and Wang 2018; Asem and Gardoni 2021; Contreras et al. 2018; Feng et al. 2020; Rosenbaum et al. 1997). Recently, Contreras et al. (2018) utilised the Bayesian regression to analyse the intact rock strength (σ_{ci}) and material constant of intact rock (*mi*) for the Hoek-Brown strength criterion and compared it with the frequentist approach. Several differences between the frequentist and Bayesian approaches from Contreras et al. (2018) are combined with other literature reviews, as summarised in Table 2. The prior distribution adopted in the analysis

by Contreras Contreras et al. (2018) is the maximum entropy principle, which allows the researcher to select the best plausible distributions. In a more advanced approach, Huang et al. (2023) employed the deep learning method, especially long short-term memory (LSTM), which yielded more reliable results in slope stability predictions compared to support vector machine (SVM), random forest (RF), and convolutional neural network (CNN).

Proposed flowcharts and case studies

The proposed flowcharts

Probabilistic empirical rock mass classifications (RMC)

As mentioned above, numerous researchers have explored rock slope stability using probability and advanced statistics. Accordingly, this research aims to develop a comprehensive design flowchart for conducting the probabilistic empirical rock mass classification. As the quantitative and empirical approaches, the output of RMCs is rock mass quality values, the steepest slope angle, rock mass friction angle, rock mass cohesion, and other rock mass strength characteristics for rock slope designs. As illustrated in Fig. 2b, seven out of ten parameters naturally yield variability values (aleatory uncertainties). In contrast, the slope angle, height, and excavation methods rely on engineers and can be considered a single value. These facts concluded that most of the input parameters in RMCs vary, leading to uncertainty in the outputs.

The probability analysis for RMCs must consider the typology of input data (discrete or continuous) of the multiparameter data. Figure 6 shows the proposed flowchart to analyse the popular RMCs using the probabilistic approach. This study merely focuses on RMR (Bieniawski 1989), SMR (Romana 1985), NSRM (Singh et al. 2013), SSAM (McQuillan et al. 2018), Q-system (Barton et al. 1974), Q-slope (Bar and Barton 2017), and GSI (Hoek and Brown 1997) rock mass classification techniques.

The final RMC probability output is the total and conditional probability for different rock mass classes or/and confidence interval (*CI*). Furthermore, Walpole et al. (2011) state that conditional probability determines the probability of a distinct group or classification range. In comparison, the *CI* describes the probability of the output falling between those values.

Probabilistic kinematic analysis

Obregon and Mitri (2019) and Rusydy et al. (2022) consider the discontinuity planes to have a variability value while the slope dimension is a fixed value. Another probabilistic kinematic approach was performed by Budetta (2020), computing the kinematic failure probability by dividing the number of potentially unstable planes by the total number of planes. However, this approach did not consider the variability of slope angles, slope directions, and friction angles. This study proposes four steps in computing the probability of occurrence (P_{tK}) in the kinematic analysis, as shown in Fig. 7.

Steps 1 and 2 are related to data processing and analysis to define the type of data distribution of observed data and prior information if the Bayesian approach is included in the probability analysis. Step 2 employs the stereography projection to determine the potential type of failure in a deterministic approach. At this step, the probability density function (PDF) of observed data and goodness of fit analysis is developed to define the statistic parameters and type of data distributions. In step 3, the probability analysis is performed by applying the kinematic conditions of each type of failure as the boundary values to determine the probability from the PDF. Step 4 starts to compute the total probability of occurrence (P_{tK}) value in series connection dealing with all probability of failures utilising Eq. 4. The P_i is the probability of each potential failure in the kinematic approach (P_{oP}, P_{oT}, or P_{oW}).

$$P_{tK} = 1 - \prod_{i=i}^{N} (1 - Pi) \tag{4}$$

The probabilistic kinematic analysis must comprehensively consider any type of failure. This study provides the methodology to calculate the total of probabilistic kinematics from possible failures. This study employs a series system with a union relationship expressed as P [p_1 U p_2 … U p_N] as Savely (1987) suggested. This approach is performed since more than one type of failure could be acted on one slope. Equation 4 is utilised to calculate the composite probability (P_{tK}) where *Pi* will be P_{oP}, P_{oW}, and $P_{oT,}$ as suggested by Obregon and Mitri (2019) and Savely (1987). The probability of occurrences for each PoP, PoW, and PoT follows the multiplication rule or product rule, where the probability only occurs when all kinematic conditions are met.

Probabilistic limit equilibrium (LE) and numerical modelling

According to Abdulai and Sharifzadeh (2021), the *PoF* is often merged with the reliability index (*RI*) or the coefficient of reliability (*CR*) analysis to quantify the rock slope stability. Shen (2012) states that *RI* is the probability of the slope in stable circumstances with certain design conditions. Identical to *PoF*, the *RI* is influenced by the variability of input values in the modelling; hence, the probability analysis of input values must be addressed as a priority.

The methodology to analyse the rock slope stability and design is shown in Fig. 8. Determining the typology of shear strength and geological conditions of the investigated rock mass is the first step of the analysis. The

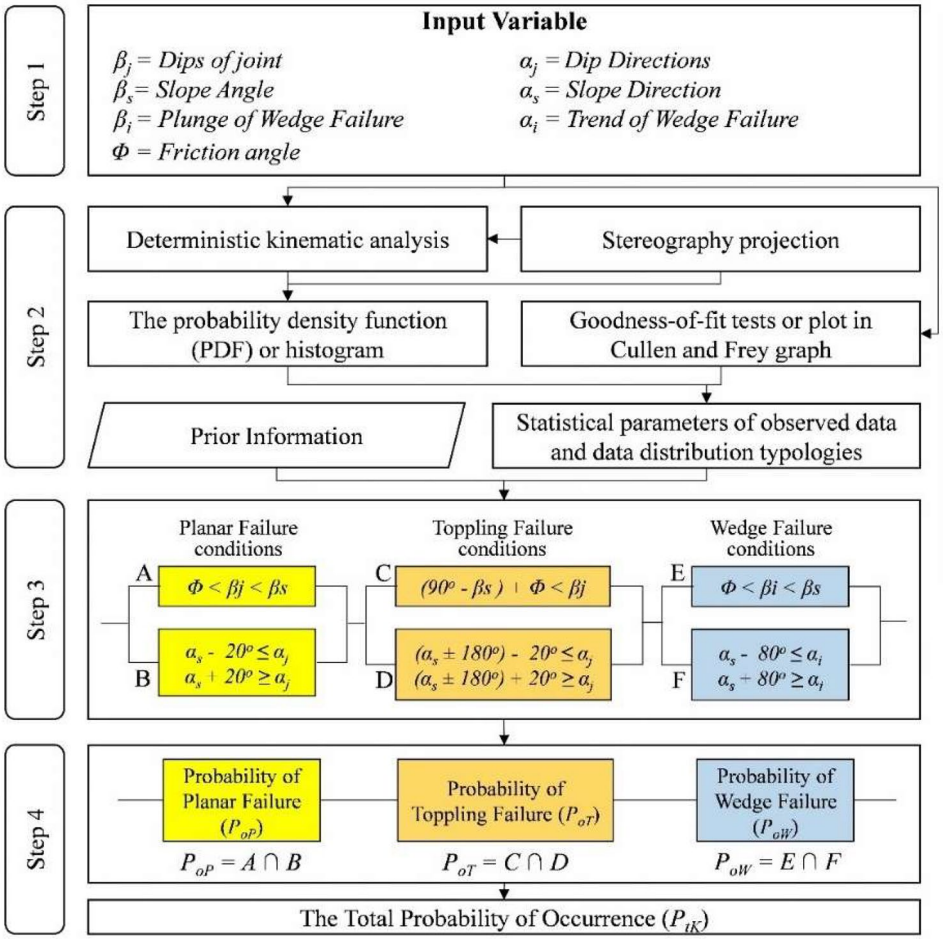

Fig. 7 The proposed flowchart to compute the total of probability kinematics (PtK) from three type failures referring to the parallel and series connection system

geological conditions will determine the type of shear strength employed in rock slope analysis.

The c and Φ are derived from the rock mass classification empirical approach known as c_m and Φ_m in the rock mass shear strength. The Hoek-Brown strength criterion is the most popular method in determining the rock mass shear strength parameters. Besides discontinuity and rock mass shear strength parameters, other input data considered in the analysis are stress, unit weight, slope geometry, joint orientation, groundwater fluctuations, external load (earthquake), and rock stratigraphy on the slope. Before probability analysis is performed, the first step is to scrutinise the type of data and basic statistical parameters of input data. In addition, the type of failure must also be recognised in kinematic analysis for the limit equilibrium method, yet the type of failure may not be required in numerical modelling.

In rock slope stability modelling, the complexity of geological structures or joints must be considered, even if it is greatly difficult to determine the accurate distribution of those structures. Singh et al. (2021) suggest employing laser scanning techniques to identify structural discontinuity automatically or utilising the photogrammetry techniques as Chen et al. (2016) conducted. Furthermore, the rock slope probability analysis needs to consider the stochastic dynamic effect of earthquake (Huang and Xiong 2017; Huang et al. 2022a, b) and groundwater fluctuation following the rainfall duration and intensity(Hussin et al. 2024; Yang et al. 2023). The earthquake model approach, as conducted in our previous research (Rusydy et al. 2017, 2018a, b, 2020b) can be employed in generating the earthquake model from the nearest fault system.

The external load, like earthquakes, exhibits variability in strength, frequency, and duration, even for earthquakes recorded in the same location (Huang and Xiong 2017; Huang et al. 2022b). Hence, adopting a probability-based approach to quantify the variability of earthquake parameters will produce a reliable estimate of slope stability under seismic load (Hu et al. 2022). Furthermore, the slope stochastic dynamic method is robust, considering non-linear stochastic seismic dynamic of slope

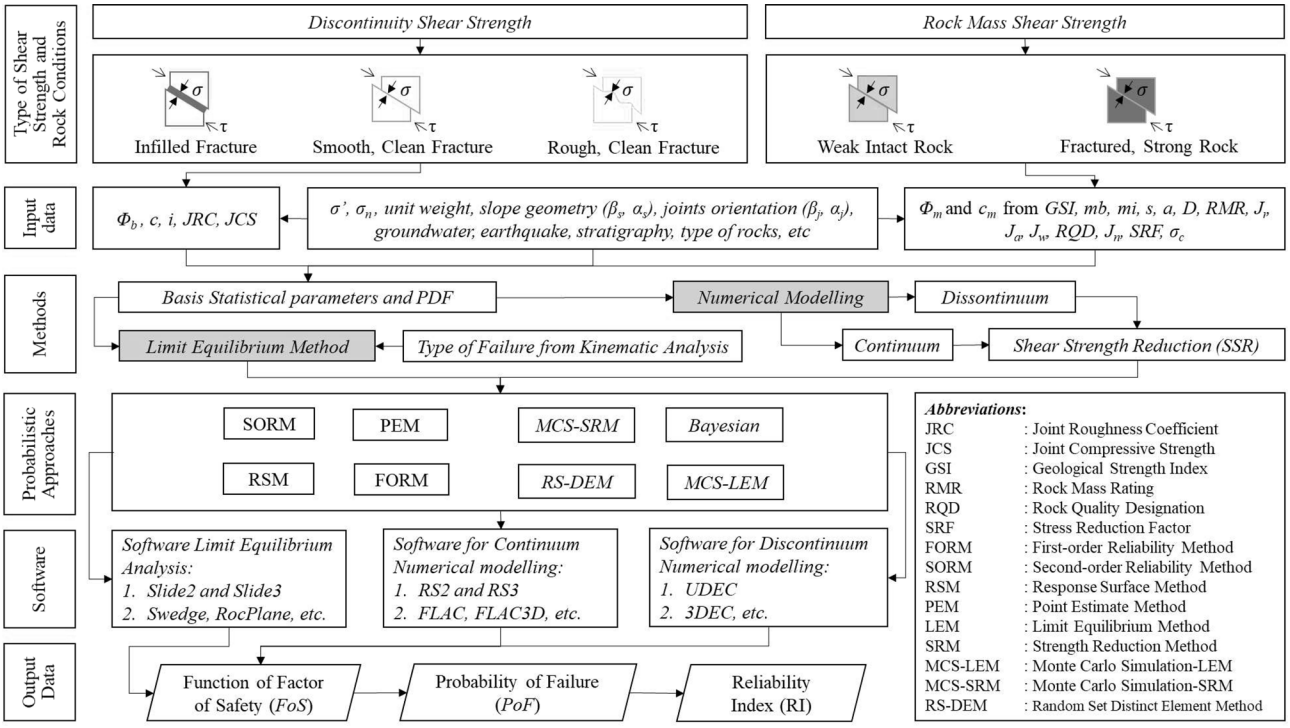

Fig. 8 The proposed flowchart to compute the probability of failure (PoF) and Reliability Index (RI) from Limit Equilibrium and Numerical modelling for rock slope stability analysis and design

compared to pseudo-static and Newmark sliding block approaches (Huang et al. 2022b).

Case studies using the proposed methodology flowchart

Geological setting of a case study slope

The proposed flowcharts in Figs. 6 and 7, and Fig. 8 are applied to one of the stable slopes in Aceh province, Indonesia. All the data are extracted from Rusydy et al. (2020a). The investigated slope is 10 km from the Great Sumatra Fault (*GSF*), as illustrated in Fig. 9. The slope is formed by argillaceous limestone, a part of the Woyla group formed during the Jurassic to early Cretaceous (Adhari and Hidayat 2023; Barber 2000; Barber and Crow 2005; Wajzer et al. 1991). According to Rusydy et al. (2019), the limestone of the Woyla group is highly fractured, bedded, disturbed-folded, and blocky due to tectonic forces from the subduction zone and GSF. At this rock slope, four rock slope stability methods are applied and discussed in the following sections.

Implementing the flowcharts

a. Probabilistic Kinematic Analysis

The dip and dip directions of joints, slope orientation, and friction angle shown in Fig. 10a were extracted from Rusydy et al. (2020a) and replot using Dips software from Rocscience. Two possible failures can occur: planar failure from joint set 1 (*J1*) and wedge failure due to the intersection plane between *J1* and joint set *J2*. However, Rusydy et al. (2020a) conducted the kinematic analysis with a deterministic approach. As stated in step 2 in Fig. 7, the goodness-of-fit test must be performed to determine the type of data distribution of observed dip angles and dip directions for both *J1* and *J2*, as denoted in Fig. 10bc. The goodness-of-fit test analysis utilises the fitdistrplus R programming package developed by Delignette-Muller and Dutang (2015). The test shows that the log-normal distribution is fit for dip angles of both joint sets and normal distribution for dip direction. The log-normal and normal distributions for observed dip angles and dip direction data identify the statistic parameters employed in the Monte Carlo simulation.

The PDF of 10,000 simulated random values and the boundary value (e.g. Φ, β_s) determine the probability of each condition, as shown in Fig. 11. After performing the Monte Carlo simulation, the probability for each condition is determined using the PDF and their corresponding boundary values. As for planar failure, the probability of the first condition, i.e., $\Phi<\beta_j<\beta_s$, is 0.707 (70.7%), as shown in Fig. 11a. It means that 7070 from 10,000 simulated dips (β_j) fall between the friction angle (Φ) and the slope angle (β_s). In other words, the probability of meeting the first condition for planar failure, where $30^o<\beta_j<66^o$ is 70.7%.

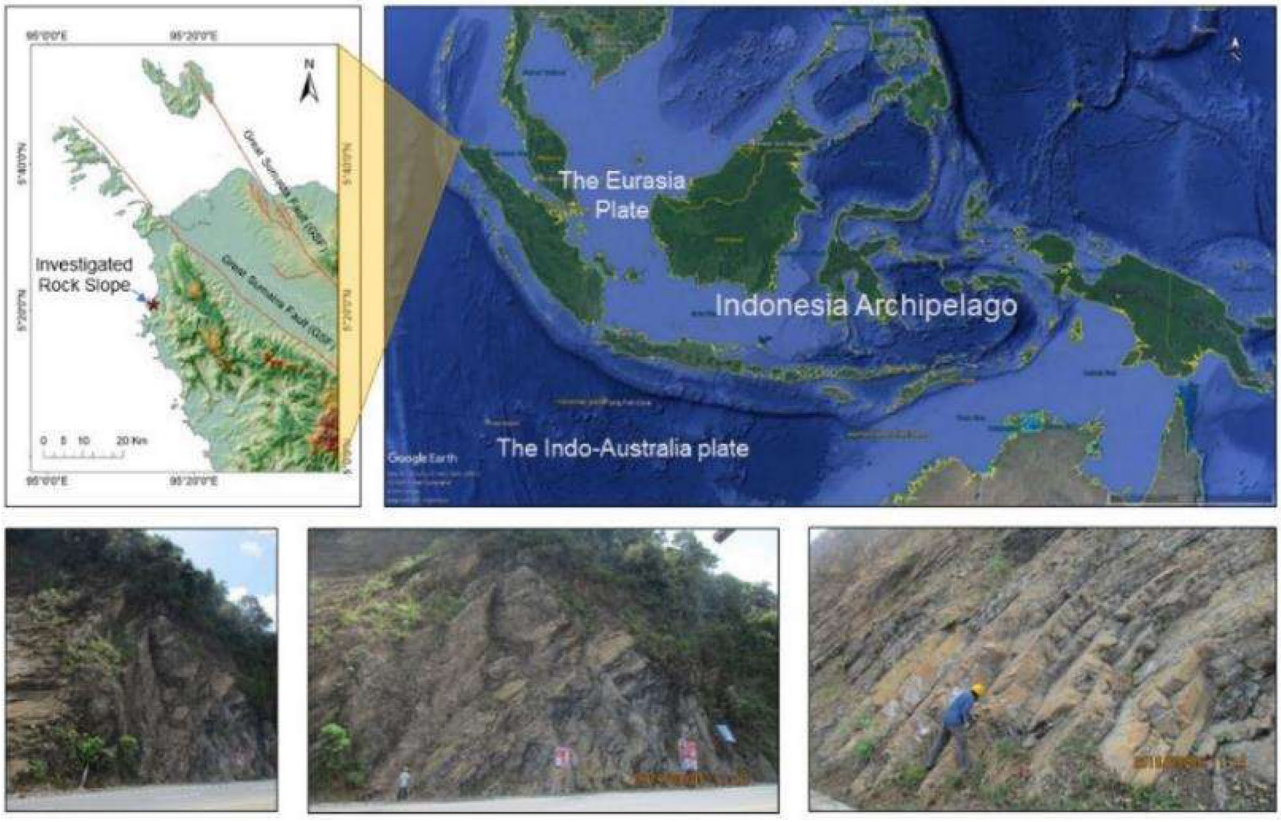

Fig. 9 The location of the investigated slope in Aceh Province, Indonesia

The second condition for planar failure involves the probability of the dip direction of the planar plane (α_j) being within 20° of the slope face (α_s=*N 268°E*). This condition is mathematically expressed as $\alpha_s - 20° \leq \alpha_j \leq \alpha_s + 20°$, which simplifies to $248° \leq \alpha_j \leq 288°$. The probabilistic analysis from the PDF reveals a value of 0.103 (10.3%), as shown in Fig. 11b.

Another possibility of failure is a wedge from the intersection of joint set 1 (*J1*) and joint set 2 (*J2*). The plunge (β_i) and trend (α_i) are calculated from random values of dips and dip directions of *J1* and *J2*, which are identified as β_{J1} and β_{J2} in the equation of Fig. 11e. In wedge failure, the first condition is like a planar failure where $\Phi < \beta i < \beta s$; accordingly, the plunge of wedge failure probability is 0.998, as shown in Fig. 11c. Furthermore, the trend (α_i) is within 80° of the slope face (α_j) in the second condition. The probability analysis from the PDF of trend (α_i) distributions reveals 1, as shown in Fig. 11d. It means all 10,000 simulated trends (α_i) are within 80° of the slope face, as shown in Fig. 11b.

The planar and wedge failures only occurred when they met the Step 3 requirements in Fig. 7. The calculation of each probability of planar failure (P_{oP}) and probability of wedge failure (P_{oW}) employs the intersection relationship (∩), where all conditions are required for slope failure. Accordingly, the probability of the first condition multiplies by the second condition for each failure. If one condition has a zero probability, P_{oP} or P_{oW} results are 0 (failure will not occur). For instance, in planar failure, if the $\Phi < \beta_j < \beta_s$ is 0.707, and the dip direction (α_j) within 20° of slope face (α_s) is 0. As a result, the probability of occurrence (P_{oP}) is 0. The probability analyses reveal that the P_{oP} and P_{oW} values are 0.074 and 0.998 sequentially. The method to calculate P_{op} and P_{oW} can be seen in steps 3 and 4 of Fig. 7.

b. Probabilistic Empirical Rock Mass Classifications

The Q-slope method from Bar and Barton (2017) was selected to determine a steeper slope's confidence interval (*CI*). The Q-slope is an updated version of the Q-system from Barton et al. (1974). Nevertheless, this Q-slope focuses on empirical analysis of rock slope stability, and the final output of this Q-slope is the possible steeper slope.

As mentioned in the previous section, the analysed rock slope is located in Indonesia and has wedge failure potential from planes J1 and J2. Rusydy et al. (2020a) employed the scanline method to determine the joint condition, orientations, and spacing. The scanline length is 71 m and is divided into seven sections, as shown in Table 3. Different sections reveal different joint numbers

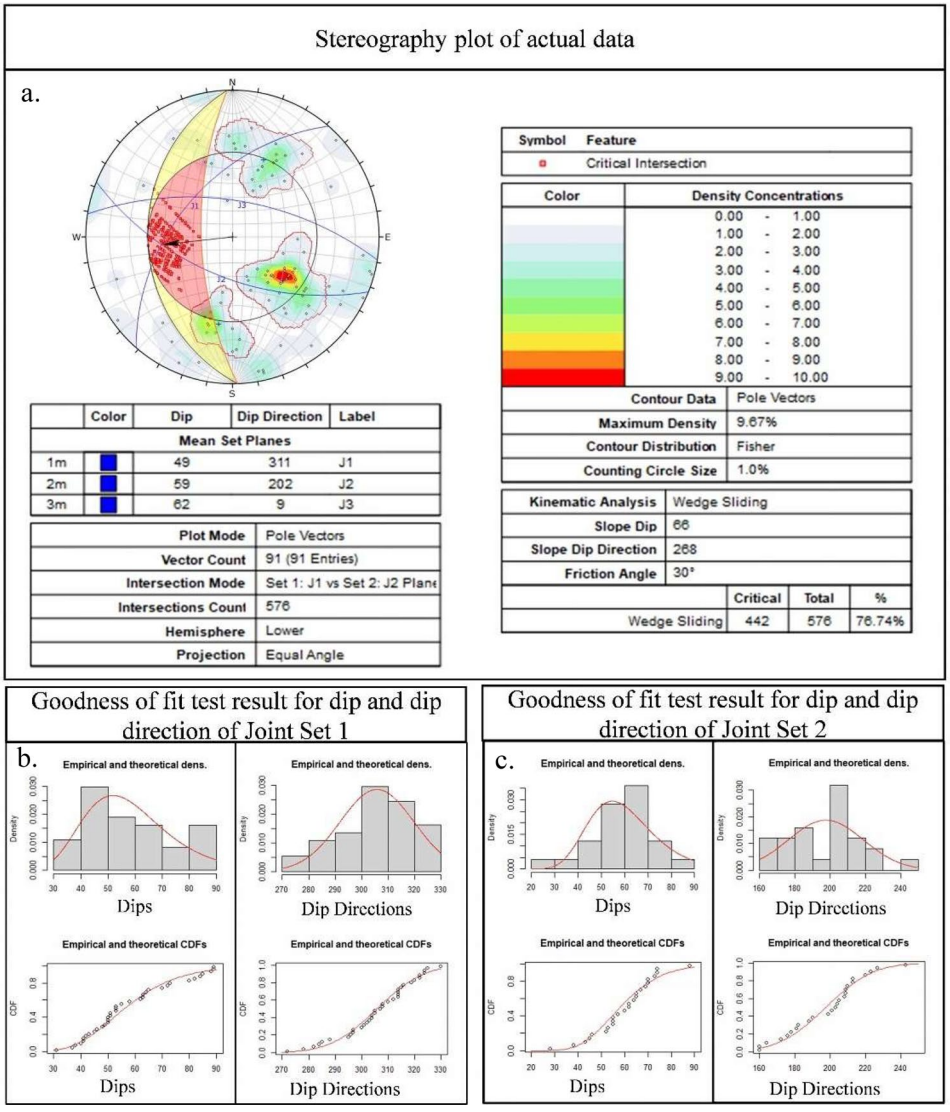

Fig. 10 (**a**) The Stereography projection of observed dips from Rusydy et al. (2020a), (**b**) the dip orientations and the goodness-of-fit test for joint set 1 (J1), (**c**) joint set 2 (J2)

(*N*), and in each section, the joint frequencies (λ) are defined to calculate the *RQD* values employing Priest and Hudson (1976) equation. The value of the joint set number (*Jn*) is taken from Bar and Barton (2017) and varies in different sections. The Q-slope parameters are the discrete data developed by Bar and Barton (2017) in the ranking range. Nevertheless, in this research, those discrete rankings are believed to have continuous data conditions; hence, those discrete rankings can be justified.

As for joint roughness number (*Jr*), only joint set 1 (*J1*) and joint set 2 (*J2*) are utilised for statistical property analyses. A similar approach is applied for joint alteration number (*Ja*), where some joints are slightly altered (*Ja* value is 2) while others have thin clay filling (*Ja* value is 8). The last parameter in the Q-slope is the Stress Reduction Factor (SRF_{slope}), consisting of SRF_a, SRF_b, and SRF_c. Only the most adverse *SRF* is employed in Q-slope calculations. According to Bar and Barton (2017), the SRF_a describes the rock slope's physical condition, while the SRF_b relates to the slope stress/strength ratio. The SRF_c defines the present of major discontinuity like a fault. In this case study, the slope has disturbances due to mechanical excavation during construction (SRF_a value is 2.5), and some rock blocks are loose and vulnerable to weathering (SRF_a value is 5). The slope stress and strength are 2.9 MPa (at 120 m depth and using a unit weight of 0.024 MN/m^3 and 74 MPa (UCS (σ_c), respectively; thus, the ratio of σ_c/σ_1 is 25.7 and categorised as a high stress-strength range (SRF_b value is 2.5–5). No fault is present in this slope; thus, the value of SRF_c is 0.

According to Bedi (2013), the *RQD*, *Jr*, and other parameters can be considered as triangular distribution

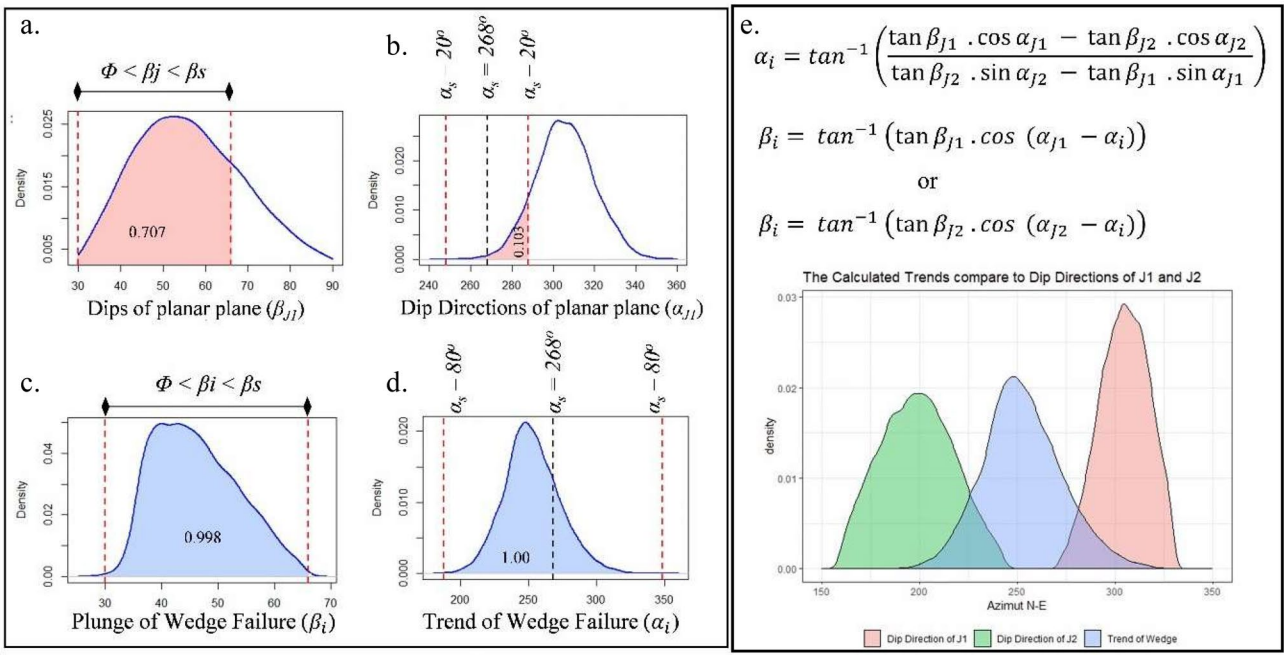

Fig. 11 The simulated probability density functions and their probabilities according to kinematic conditions of planar and wedge failures, (**a**) the PDF of dip of planar plane, (**b**) the PDF of dip direction of planar plane, (**c**) the PDF of plunge of wedge failure, (**d**) the PDF of trend of wedge failure, (**e**) the equations in calculating the trend and plunge, and the PDF of calculated trend compare to dip directions

Table 3 The input parameters for Q-slope probabilistic analysis

Parameters/Sections	Dist. (m)	*N*	λ	RQD	Jn	Jr-J1	Jr-J2	Ja-J1	Ja-J2	SRFa	SRFb
Section 1	9.9	9.0	0.9	90.9	4.0	Jr distribution at *J1* based on field data, total data are 37	Jr distribution at *J2* based on field data, total data are 25	Slightly altered joint wall, softening or low friction clay mineral coating, softening, clay mineral filling		Disturbance from excavation, loose block, susceptibility to weathering	The height of the slope is approximately 120 m, with a high stress-strength range, $\sigma_c/\sigma_1 = 25.7$
Section 2	10.0	15.0	1.5	85.2	6.0						
Section 3	9.9	20.0	2.0	80.2	4.0						
Section 4	10.1	16.0	1.6	84.4	12.0						
Section 5	11.4	14.0	1.2	87.8	3.0						
Section 6	11.0	10.0	0.9	91.0	6.0						
Section 7	8.8	7.0	0.8	92.1	6.0						
Minimum values				*80.23*	*3.00*	*2.00*	*1.50*	*2.00*	*2.00*	*2.50*	*2.50*
Maximum values				*92.09*	*12.00*	*4.00*	*4.00*	*8.00*	*8.00*	*5.00*	*5.00*
Mode values				*87.00*	*88.00*	*3.00*	*2.00*	*4.00*	*4.00*	*3.75*	*3.75*
Mean values				*87.37*	*5.86*	*2.76*	*2.48*	-	-	*3.75*	*3.75*
Standard Deviation				*4.01*	*2.75*	*0.71*	*0.74*	-	-	-	-

in the Q-system, and the input values for simulations are minimum, maximum, and mode values for each parameter, as shown in Fig. 12a – g. 10,000, 100,000, and 1,000,000 random values in Monte Carlo simulation using the *EnvStats* package developed by Millard (2013) in *R* programming software for triangular data distribution. The results of 10,000 random values for each parameter are shown in Fig. 12a – g. In this slope, two discontinuity planes are favourable; hence, the values are 1. Furthermore, this analysis assumes that it occurs in a wet environment, and the slope has unstable geological structure conditions; as a result, the J_{wise} value is 0.6.

Figure 12h shows the results of the variability of Q-slope output values in relative frequency histogram and PDF driven by the variability of input parameters. The type of Q-slope data distribution is a log-normal distribution, as revealed from fit distribution using the Cullen and Frey graph and Goodness-of-fit tests, as shown in Fig. 13a, b. This finding has a similar pattern distribution of the Q-system at the Shimizu tunnel in Japan (Lu et al. 2022). The final output of the Q-slope is the steeper slope angle (β) calculated utilised in the equation denoted in Fig. 12. According to Bar and Barton (2017), that equation merely applies to the slope angle between 35° to 85°.

Figure 12i shows the final output of the steepest slope angle (β). The data distribution of the steepest slope angle (β) is normal distribution as revealed from the fit distribution test (see Fig. 13c, d). The point estimate method

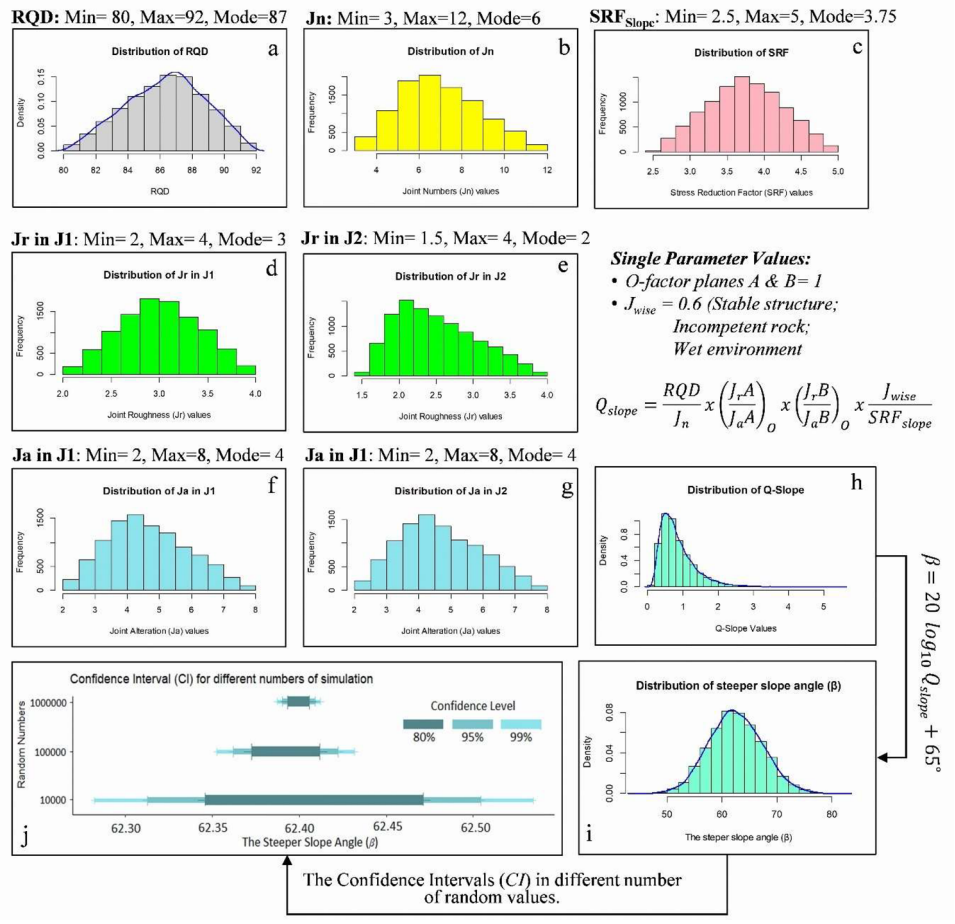

Fig. 12 The result of example probability analysis for Q-slope rock mass classification at investigated slope in Aceh Province, Indonesia

(PEM) determines the normal distribution data's confidence interval (*CI*). Hence, calculating the *CI* employs the PEM approach; the results for a different number of random values are shown in Fig. 12j. This Figure indicates that the *CI* for 80%, 95%, and 99% of the steepest slope angle (β) declined significantly as the number of random values increased. Most statistical analyses commonly use a *CI* of 95%. Thus, the probabilistic Q-slope analysis concludes that the steepest safe slope angle (β) for slope design must be between 62.31° – 62.50° for 10,000 random values. This approach may be implemented in other rock mass classification techniques using the proposed flowchart in Fig. 6.

c. Probabilistic Limit Equilibrium (LE)

A case study from a slope in Indonesia using the limit equilibrium (*LE*) method is presented in this section. The previous kinematic analysis reveals that the wedge failure appeared to occur due to the intersection of joint set 1 (*J1*) and joint set 2 (*J2*). Furthermore, the probabilistic kinematic analysis in the previous section reveals a 99.8% likelihood of a wedge failure (see Sect. 5.2.2a). A multitude of rock properties is employed in probabilistic LE analysis. Table 4 presents the input parameters. This table shows that some input parameters are distributions, while single values represent others due to a lack of data. The distribution of *FoS* is determined by utilising Swedge software from Rocscience.

The Swedge software is used to determine the *FoS* and *PoF* of a wedge failure using the LHS method to generate the random input values. In this case, the Psych R programming package developed by Revelle and Revelle (2015) plots the correlation of inputs and outputs in probabilistic *LE* simulation from the Swedge program. Regarding the failure mechanism, the wedge failure occurs in this rock slope due to the intersection of two discontinuity planes (*J1* and *J2*); thus, the Barton and Bandis (1982) failure criterion is employed in the analysis. The *FoS* of 1.5 is utilised as the reference value or safety limit between non-stable and stable areas because the case study is a rock-cut beside a highway (civil engineering project).

This study conducts sensitivity analysis for six related input dips, *JRC*, normal stress, shear strength, plunge and safety factor (*FoS*). As presented in Fig. 14a, the

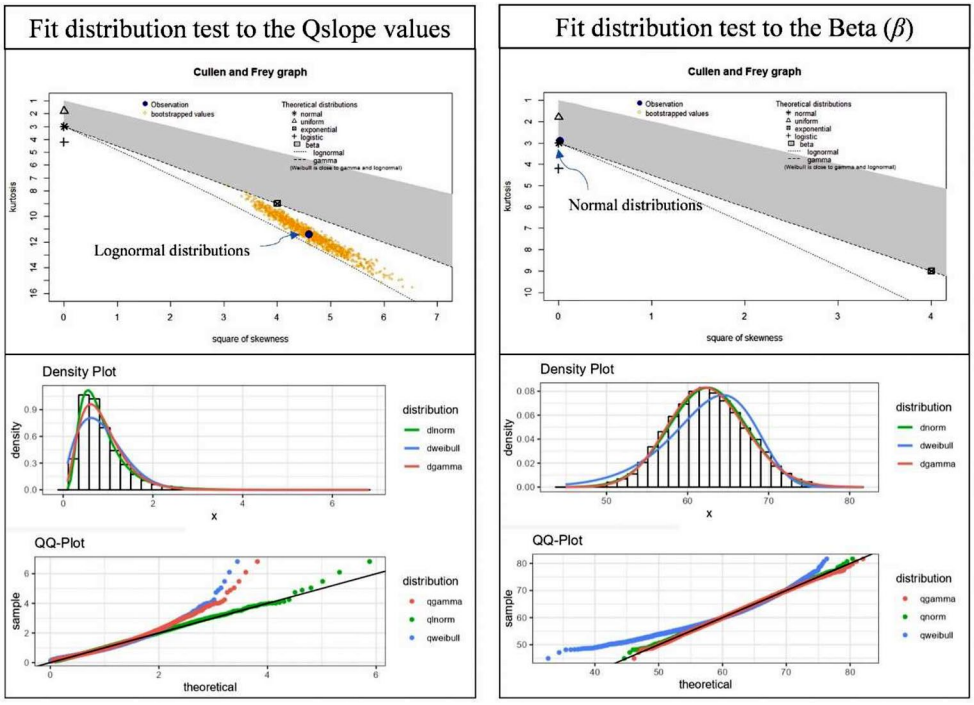

Fig. 13 Fit distribution test results for the Q-slope and steepest slope (β). The fitdistrplus and Fitur R programming packages are employed in this analysis

Table 4 The input parameters used in limit equilibrium analysis for wedge failure

Parameters		Statistic distributions	Mean	SD	Relative min	Relative max
Slope (Lower Face)	Slope Angle (°)	-	66	-	-	-
	Slope Face (°)	-	268	-	-	-
	Height (m)	-	60	-	-	-
	Bench width (m)	-	100	-	-	-
Slope (Upper Face)	Slope Angle (°)	-	36	-	-	-
	Slope Face (°)	-	268	-	-	-
Joints orientations for Wedge Failure	Dip of Joint 1 (°)	Truncated LogNormal	58.22	16.51	31	89
	Dip of Joint 2 (°)	Truncated LogNormal	59.6	13.16	28	88
	Dip Direction of Joint 1	Truncated Normal	305	13.95	272	330
	Dip Direction of Joint 2	Truncated Normal	197	21.29	160	243
Joint Strength: Barton-Bandis	JRC for Joint 1	Normal	10	4	2	16
	JRC for Joint 2	Normal	10	4	2	16
	JCS for Joint 1 (MPa)	-	39	-	-	-
	JCS for Joint 2 (MPa)	-	39	-	-	-
	Friction Angle (°)	-	30	-	-	-
	Friction Angle (°)	-	30	-	-	-
Joint Water Pressure	Hu	Exponential	0.003	-	0	1
Seismic Force	Seismic Coefficient	-	0.1	-	-	-

plunge (βi) has a high influence on *FoS* followed by JRC and shear strength Four scenarios, as shown in Fig. 14b-e, have been developed. The values of *PoF* increase as the groundwater and lateral load from the earthquake are incorporated into the models. The consequence of groundwater filling the discontinuity planes on the *PoF* value is lower than the seismic load. Hence, this study neglects the groundwater and compares the two scenarios with or without seismic load, as denoted in Fig. 14f.

This rock slope case study is approximately 10 km from the Aceh segment of the Great Sumatra Fault (GSF) system. According to Ito et al. (2012); Rusydy et al. (2020b), the Aceh segment of GSF can generate earthquakes up to 7 Mw (moment magnitude); hence, this rock slope can be subjected to significant seismic load. According to national seismic hazard maps of Indonesia developed by Irsyam et al. (2020), for 1-second spectral accelerations and a 2% probability of exceedance in 50 years, the peak

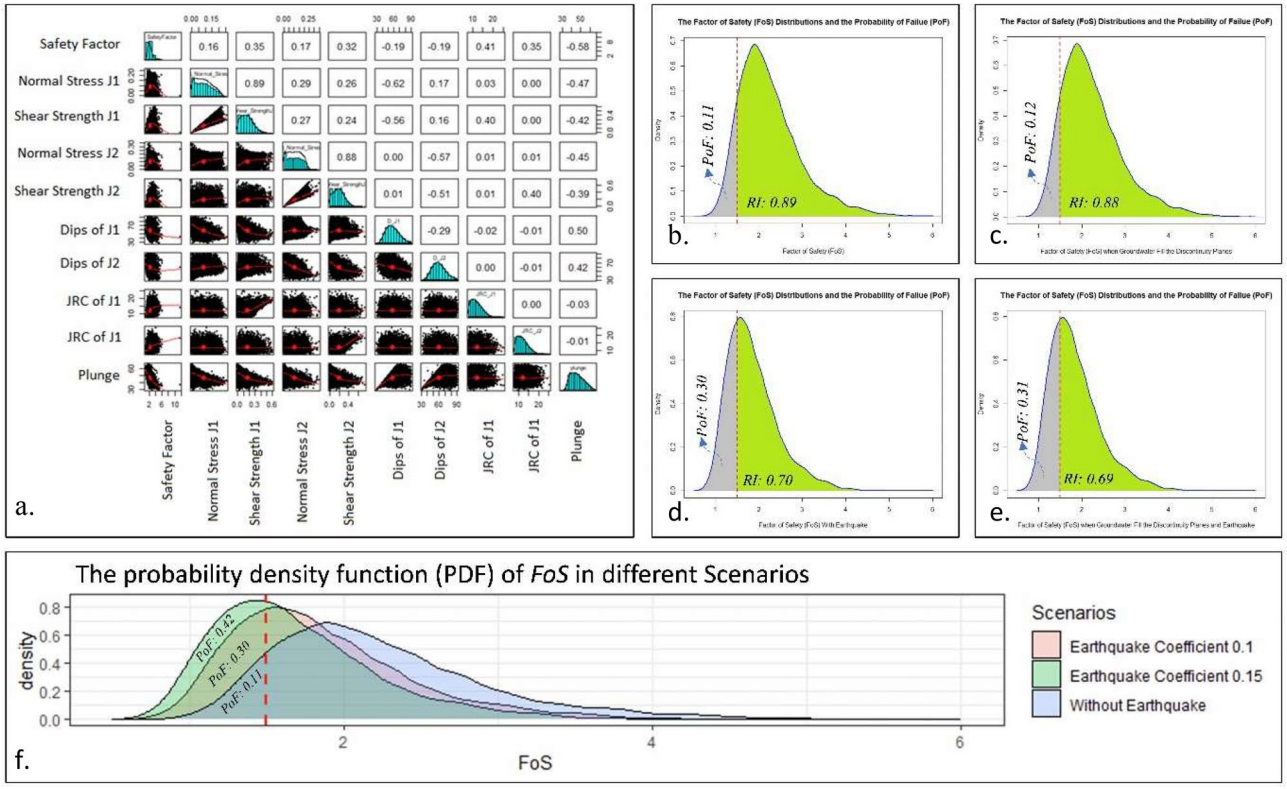

Fig. 14 The example results of probabilistic limit equilibrium analysis for wedge failure (**a**) The correlation between inputs and outputs, (**b**) The PoF and CR when the slope free from groundwater and earthquake, (**c**) The PoF and CR when the groundwater fills the discontinuity planes without earthquake, (**d**) The PoF and CR when load by the earthquake without groundwater, (**e**) The PoF and CR with groundwater and earthquake lateral load. (**f**) The PDF of FoS different earthquake scenarios

Table 5 The input parameter for numerical modelling

Properties/Parameters	Type/Values
Failure criterion	Jointed Generalised Hoek Brown (*GHB*) and Generalised Hoek Brown (*GHB*)
Slipe criterion	Barton – Bandis
Elastic Type	Isotropic
Material Type	Plastic
Unit Weight (MN/m^3)	0.024
Poisson's Ratio	0.25
Young's Modulus (MPa)	20,700
UCS (MPa)	74
Normal Stiffness (MPa/m)	21,290
Shear Stiffness (MPa/m)	3400
GSI	54 refer to Rusydy and Al-Huda (2021)
Porosity	0.1
Average spacing (meter)	0.8
Average Length of a joint (meters)	10
Plunge/Dips	Min: 40°, Mean: 46°, Max: 51°
JRC	Min: 12, Mean: 13, Max: 14
Residual Friction Angle	Min: 27.2°, Mean: 29.5°, Max: 32.0°
Type of Joint Networks	Parallel Deterministic

ground acceleration (PGA) in this rock slope is between 0.4 and 0.5 g. Referring to Bray and Travasarou (2009), the 0.4–0.5 g of a 1-second ground motion period will yield 0.1–0.15 horizontal inertial force of seismic coefficients. The simulation shows that the *PoF* is 0.11 without the earthquake load; nevertheless, the *PoF* increases to 0.30 as it is loaded by 0.1 earthquake coefficient in the second scenario. In the thirst scenario with an earthquake coefficient of 0.15, the *PoF* elevates to 0.42, and the slope becomes unstable.

d. Numerical Modelling

The same slope is also analysed using numerical modelling. The RS2 software from Rocscience is employed in the analysis, allowing input of the joint elements. The RS2 is a finite element method (FEM) applying the strength reduction method (*SRM*) to determine the *FoS*. The critical Strength Reduction Factor (*SRF*) revealed from the RS2 simulation determines the *FoS*. According to Hammah et al. (2008), including the joint element in continuum-based FEM produces reliable results, and this approach can capture the scale effect in discontinuous

rock masses. The input parameters and the adopted strategies in the modelling are shown in Table 5.

The RS2 provides the probabilistic outputs by generating numerous random outputs through the PEM, MCS, and Latin Hypercube approaches. Nevertheless, activating those options requires more time and a high-performance computer for data processing. Instead of using those approaches, this study employs PEM to determine the range of value of 95% of *CI* for three significant input parameters (Plunge/Dips, JRC, and Friction Angle) in modelling. The sensitivity analysis in the previous section reveals that plunge/dips of joint and JRC highly influence the output. This PEM incorporates Box-Behnken Design (BBD) to calculate the second-order polynomial in estimating the response function. In the BBD approach, the input variables are randomly developed into three levels of values: (-1) as the minimum value, (0) as the mean value, and (1) as the maximum value.

Accordingly, 78 models are developed in different combinations of input values on three different scenarios and two failure criteria, jointed and homogenous GHB. The *FoS* results obtained from the runs/simulations are presented in Table 6; Fig. 15. BBD's minimum and maximum input values are calculated from PEM (95% CI) analysis from their distributed data of dips/plunge, JRC, and residual friction angle (Φ_r). The slope geometry and the results of rock slope numerical modellings are illustrated in Fig. 15. Regarding seismic load, this study employed pseudo-static seismic coefficients of 0.1 and 0.15 for simplification purposes.

The goodness-of-fit tests are performed to determine the type of data distribution of *FoS* in different scenarios. The results for the goodness-of-fit test reveal that the log-normal data distribution is suitable for *FoS* in the following scenarios: dry conditions without earthquakes, earthquake coefficient 0.1, and earthquake coefficient 0.15. The MCS generates 10,000 random values of *FoS* for each scenario based on the statistical parameters of *FoS*'s results. This simulation reveals the *FoS* data distribution in different scenarios and its *PDF*, as denoted in Fig. 16d. Different failure criteria reveal different results of *FoS*, as illustrated in the boxplot in Fig. 16a. More details are explained in discussion section.

Discussion

This study has developed the flowchart of probability method for four slope stability methods (see Figs. 6 and 7, and Fig. 8) for more detail. In all probabilistic processes, it is emphasised that developing the stochastic model and determining the typology of data distribution for rock properties are crucial steps for both frequentist and bayesian statistic approaches. Therefore, the selection of data distribution type must be made based on previous studies and validated through the goodness-of-fit

Table 6 The result of *FoS* in different scenarios of BBD's patterns and slope conditions

Run Order	BBD's Patterns	Running Parameters Based on BBD's Pattern and PEM			FoS from Numerical Modelling in different Failure criteria and scenarios					
					GHB and Joint Network			Jointed GHB and Joint Network		
		Plunge/ Dips (°)	JRC	Φ_r(°)	Dry	Seismic Coeff. (0.10)	Seismic Coeff. (0.15)	Dry	Seismic Coeff. (0.10)	Seismic Coeff. (0.15)
1	-1 -1 0	40.0	12.0	29.5	2.24	1.91	1.75	1.82	1.50	0.91
2	1–1 0	51.0	12.0	29.5	2.30	1.90	1.75	1.74	1.11	1.30
3	-1 1 0	40.0	14.0	29.5	2.30	1.98	1.75	1.87	1.57	1.39
4	1 1 0	51.0	14.0	29.5	2.39	2.02	1.86	2.00	1.66	1.58
5	-1 0–1	40.0	13.0	27.2	2.28	1.96	1.75	1.69	1.35	0.90
6	1 0–1	51.0	13.0	27.2	2.24	1.88	1.79	1.44	1.08	0.99
7	-1 0 1	40.0	13.0	32.0	2.30	1.96	1.77	1.82	1.50	0.99
8	1 0 1	51.0	13.0	32.0	2.30	1.95	1.73	1.87	1.27	1.13
9	0–1 -1	46.0	12.0	27.2	2.25	1.94	1.70	1.64	1.02	1.02
10	0–1 1	46.0	12.0	32.0	2.34	1.94	1.75	1.93	1.32	1.14
11	0 1–1	46.0	14.0	27.2	2.20	1.93	1.77	1.61	1.14	0.99
12	0 1 1	46.0	14.0	32.0	2.19	1.95	1.71	1.97	1.21	1.17
13	0 0 0	46.0	13.0	29.5	2.29	1.93	1.78	1.78	1.13	1.12
Statistical Parameter of *FoS* for log-normal data distributions				*Mean Log*	*0.82*	*0.66*	*0.56*	*0.57*	*0.25*	*0.10*
				SD Log	*0.02*	*0.02*	*0.02*	*0.09*	*0.15*	*0.16*
				Minimum	*2.19*	*1.88*	*1.70*	*1.44*	*1.02*	*0.90*
				Maximum	*2.39*	*2.02*	*1.86*	*2.00*	*1.66*	*1.58*
				Range	*0.20*	*0.14*	*0.16*	*0.56*	*0.64*	*0.68*

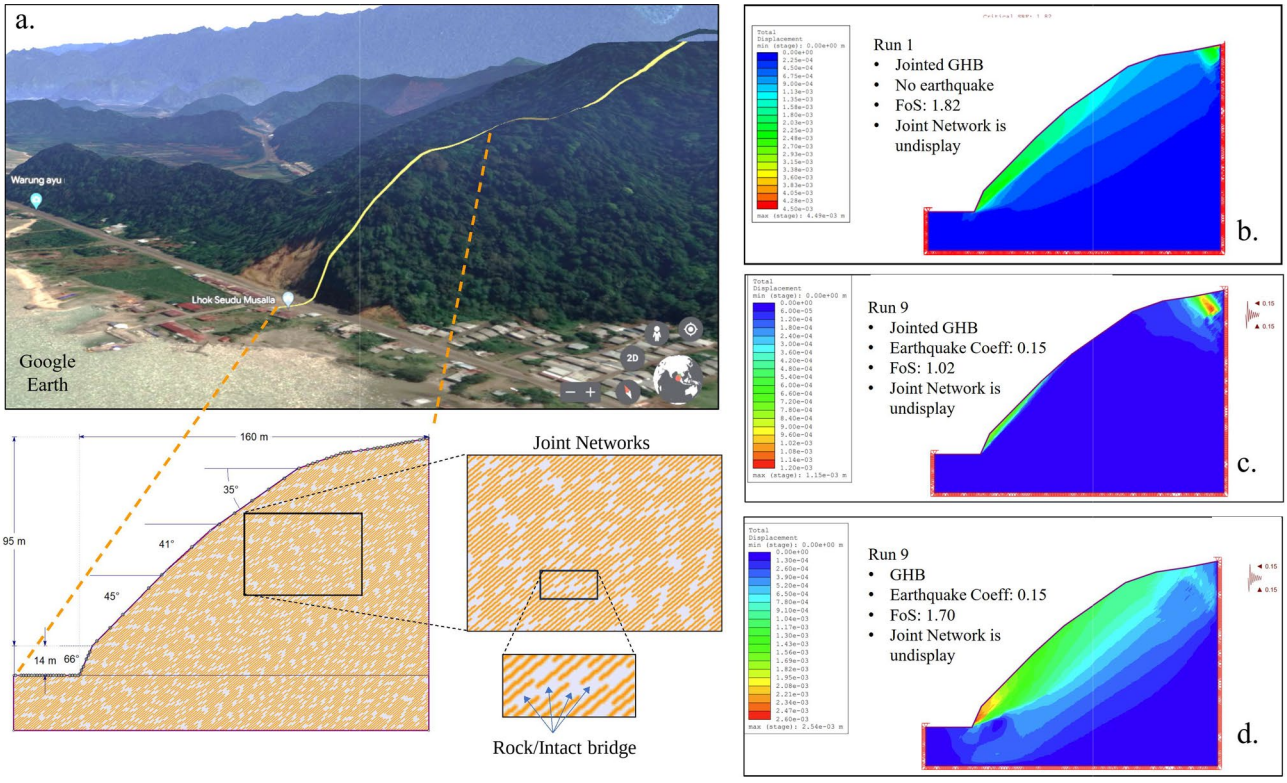

Fig. 15 (**a**) The bird's view of the investigated slope and its geometry from Google Earth. The result of numerical modelling. (**b**) Run 1 jointed GHB with no earthquake. (**c**) Run 9 Jointed GHB in 0.15 of earthquake coefficient. (**d**) Run 9 GHB in 0.15 of earthquake coefficient

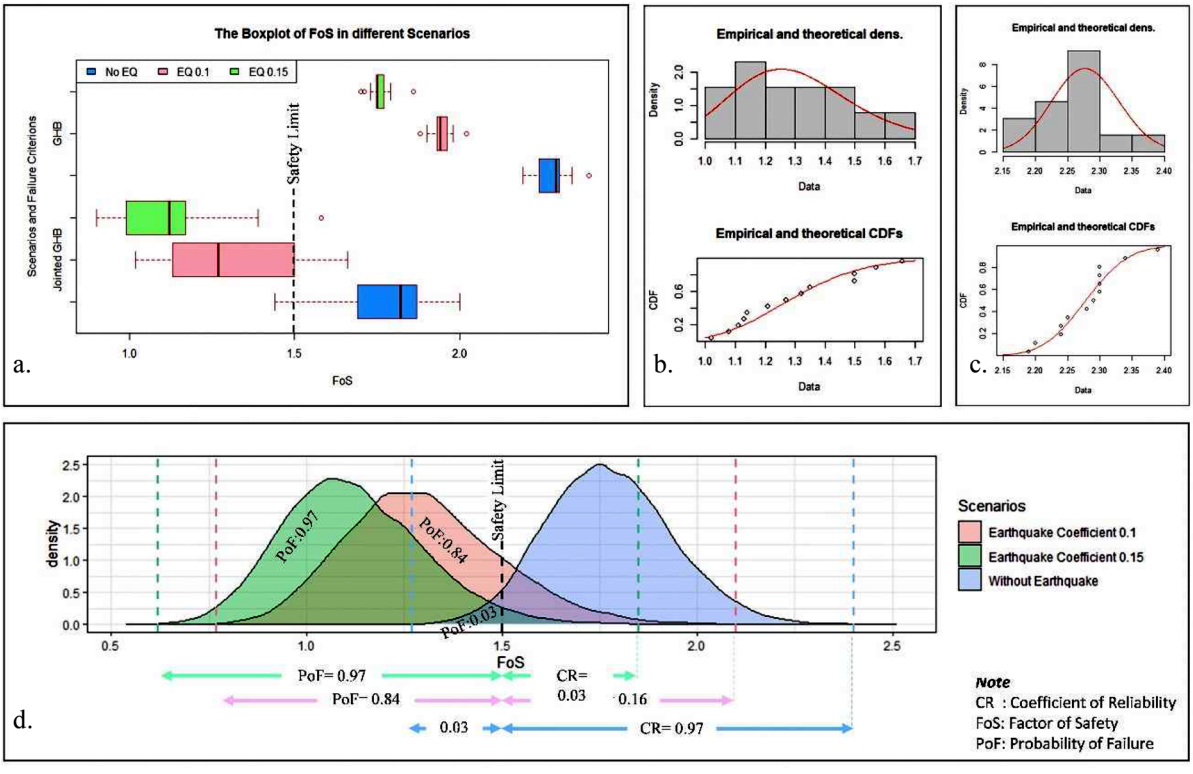

Fig. 16 (**a**) The boxplot of FoS in different scenarios from numerical modelling. (**b**) The goodness-624 of-fit test of FoS from Jointed GHB in 0.1 earthquake coefficient. (**c**) The goodness-of-fit test of FoS from GHB. (**d**) The PDF of simulated FoS for jointed GHB failure criterion in different scenarios

tests method, considering that different rock properties may follow different distribution types. Even when dealing with similar parameters, it leads to varying outcomes. The chosen data distribution type will influence the statistical parameters used in the probabilistic analysis, and each proposed flowchart presents a novel approach compared to previous studies. The following paragraphs provide a comprehensive discussion of proposed flowcharts and implementation of flowcharts.

Proposed flowcharts

In the proposed flowchart for the RMC approach, this study classifies all input variables into six groups. It is important to note that all those variables have both aleatory and epistemic uncertainties. During the data acquisitions, some data are collected as discrete data following standard rankings from established RMCs, such as the joint number (*Jn*), joint roughness (*Jr*), and joint alteration (*Ja*) in Q-system and environment condition (J_{wise}) Q-slope classifications, and various others discrete parameters. This study recommends converting the discrete data to continuous data employing continuous functions equations, either developed in previous research or new continuous functions.

Probabilistic kinematics assumes each failure has probabilities depending on the dip, dip direction, and friction angle variabilities. These variables are considered independent because no correlations have been found among them. Accordingly, the multiplication rule is applied in calculating the probabilities of different failure types. The proposed flowchart in Fig. 7 provides a comprehensive and systematic approach to conducting probabilistic kinematic analysis. The proposed flowchart quantifies all kinematic conditions for planar, wedge, and toppling failures mathematically and illustrates how probability calculations are performed in detail.

The Monte Carlo Simulation (MCS), Point Estimate Method (PEM), Bayesian analysis, and Markov Chain Monte Carlo (MCMC) are the most used probabilistic approaches for input variables in both Limit Equilibrium (LE) and numerical modelling. In some cases, these methods are combined with techniques such as FORM (first-order reliability method), SORM (second-order reliability method), response surface method, and RS-DEM (random set district element method). In addition, the LE method requires providing the type of failure from kinematic analysis. In comparison, FEM numerical modelling does not require this input.

Implementation of flowcharts

Furthermore, implementing the proposed probabilistic analysis in four different methods yields varying results, as found in the case study where the proposed flowcharts were implemented. Here, we discuss the critical findings from implementing these proposed flowcharts.

In kinematic analysis, both planar and wedge failures can occur independently. Therefore, those failures have union connections (U), and the series system is applied, as noted in Eq. 4. Dip and dip direction, plunge, as well as trend, are independent variables. Hence, the multiplication rule is applied to compute the value probabilities of failure. Notably, this probability value does not represent the overall probability of failure for this slope, which is 0.998 (99.8%). Instead, it determines the likelihood of specific types of failure occurring, which is relevant to the risk perspective in the investigated slope.

Due to its recent applicability in civil and mining engineering projects, the proposed research flowchart for rock mass classification has been implemented to Q-slope. The safe steepest slope angle (β) variability resulting from probabilistic analysis is represented in confidence interval (see Fig. 12j). Nevertheless, the distribution of β values in Fig. 12i falls within 50° – 80°. This result supports field observation that the slope angle is 66° and the slope remains stable. Therefore, this outcome confirms the reliability of the Q-slope analysis in tropical countries, and the probability analysis of the Q-slope provides a range of β values. Additionally, Q-slope probability analysis offers engineers a wider range of slope angles (β) to choose from before starting excavation or slope development, whether in civil engineering or mining projects.

The LE and FEM numerical modelling are conducted under various scenarios and failure criteria. The LE analysis indicates stable conditions under dry and saturated conditions without an earthquake load (see Fig. 14bc). This outcome is consistent with observations made in the field. Further analysis revealed that the LE method predicted an unstable slope when seismic loads were generated. Wyllie (2018) mentions that a slope angle of more than 25° is vulnerable to failure under seismic loads. Other factors that may influence the stability of this slope under seismic load including weathering, discontinuity characteristics, induration, and groundwater presence. It should be noted that the LE method only considers the forces acting on the slope and cannot determine the movement and stress concentration within the slope. Consequently, the LE method is limited in capturing the complexity of rock slope failure. Therefore, this research conducts numerical modelling under different failure criteria, including the general GHB and jointed GHB, as well as various earthquake scenarios.

As regard FEM numerical modelling, This *PoF* for jointed GHB numerical modelling was lower than that obtained through the probabilistic LE approach for a similar slope, specifically under dry conditions. This difference arises because the LE model employs Swedge

software and considers the wedge plane's long persistence. In contrast, FEM numerical modelling considers the "rock/intact bridge" between the joint, and it is defined in the model (see Fig. 15a for rock/intact bridge illustration). Hence, the *FoS* in the LE model tends to be lower than in numerical modelling.

In the seismic load scenarios, the *PoF* increases to 0.84 (84%) and 0.97 (97%) for earthquake coefficients of 0.1 and 0.15, respectively, in numerical modelling. These *PoFs* are significantly higher than those obtained from probabilistic *LE*, which are only 0.3 (30%) and 0.4 (40%). The results indicate that in numerical modelling using the Generalised Hoek-Brown criterion, all *FoSs* are higher than the safety limit (1.5). It implies that the slope remains stable under any circumstances and with similar input parameters. This result aligns with the findings of Sari (2019), which also noted that the jointed GHB yields lower *FoS* compared to homogenous GHB.

Another significant finding in this study is that the range of *FoS* obtained using the jointed GHB criterion is higher than the homogenous GHB criterion (refer to Table 6 and boxplot in Fig. 16a). These findings demonstrate that the jointed GHB criterion produces high uncertainty in *FoS* outputs compared to homogenous GHB, which yields low uncertainty outputs. These differences in *FoS* outputs are known as modelling uncertainty (epistemic uncertainty), which yields from the mathematical and mechanical processes employed during modelling. Distinct modelling criteria result in varying outcomes because the calculation procedure differs.

Additionally, the case example provided for numerical modelling above illustrates how aleatory uncertainty, naturally inherent in rock properties like dips, JRC, and friction angle (Φ), can be addressed. Furthermore, the example of a case study conducted with different failure criteria underscores how epistemic uncertainty is revealed in the modelling process.

Jointed and homogenous GHB reveal different results regarding the type of failure and rock displacement. In the Jointed GHB model, the slip surface follows the joint dip or plunge in wedge failure (see Fig. 15b and c). In addition, in numerical modelling with jointed GHB criterion, an altered failure surface can be observed, according to Hammah et al. (2008). In the homogeneous GHB model, the slip failure typically follows a circular pattern (see Fig. 15d). Given that, the investigated rock exhibits unfavourable joint orientation and that joints mostly control the failure mechanism. Therefore, the failure mechanism from the jointed GHB model is considered more reliable and representative of the site condition.

The total probability of failure

The final novelty of this study involves the calculation of the total Probability of Failure (*PoF*) by integrating various methodologies. The integrated probability rock slope stability analysis represents a robust approach for addressing aleatory and epistemic uncertainties. Moreover, rock slope failures in mining and civil engineering projects can significantly impact transportation connectivity and mining operations, disrupting moving vehicles and road/track blockages. The combined total *PoF* and its associated consequences collectively determine the risk of slope failure, known as Quantitative Risk Assessment (*QRA*).

The total *PoF* is calculated by multiplying the kinematic and kinetic results probabilities, as outlined by Budetta (2020); Obregon and Mitri (2019). This study presents the kinematic probability result in subsection **a**, while the kinetic probability is derived from limit equilibrium (subsection **c**) combined with numerical modelling (subsection **d**) result. Both the limit equilibrium (*LE*) and numerical modelling/Finite Element Method (*FEM*) approaches exhibit distinct methodologies for calculating the *FoS*; nevertheless, several input parameters are shared between these methods. This study considers the *LE* and *FEM* are independent and not mutually exclusive. Accordingly, the additive rule described by Walpole et al. (2011) can be applied as the union of two events or as the complement of certain events. Equation 5 expresses the calculation of the kinetic probability, and Eq. 6 outlines the computation of the total *PoF*. The summary of all conducted approaches and total *PoF* in this study as denoted in Table 7.

$$P(LE \cup FEM) = P(LE) + P(FEM) - P(LE \cap FEM) \tag{5}$$

$$Total\ of\ PoF = [P(LE \cup FEM)] \times [P(Kinematic)] \tag{6}$$

Conclusions

Mining and civil engineering projects have distinct rock slope stability and analysis requirements. This study concludes that both disciplines consider geological structures essential for slope stability. However, the degree of reliability, long-term stability, the factor of safety, and other factors have different standards. Moreover, both projects must consider the variability of rock properties as a fundamental input in slope stability analysis and design.

This study develops numerous design methodology flowcharts that serve as basic guidelines for probabilistic analysis in rock slope stability studies. Furthermore, the case studies implementing the flowchart provided in this paper demonstrate the applicability of these flowcharts to probabilistic rock slope stability studies. The results

Table 7 Summary result of four rock slope assessments and total *PoF*

No.	Methods	Probability of Occurrence for Kinematic and PoF			CI 95%
		No Earthquake	Earthquake Coeff. 0.10	Earthquake Coeff. 0.15	
1	Probabilistic Kinematic (wedge failure)	99.8%	99.8%	99.8%	-
2	Probabilistic Rock Mass Classifications (Q-Slope)/Steeper slope	-	-	-	62.31° –62.50°
3	Probabilistic Limit Equilibrium	11.0%	30.0%	42.0%	-
4	Probabilistic Numerical Modelling Jointed GHB	3.0%	84.0%	97.0%	-
5	Probabilistic Numerical Modelling GHB	0.0%	0.0%	0.0%	-
Total *PoF* for Jointed GHB		13.64%	88.62%	98.06%	-
Total *PoF* for GHB		10.98%	29.94%	41.92%	-
Coefficient of Reliability for Jointed GHB		86.36%	11.38%	1.94%	-
Coefficient of Reliability Index for GHB		89.02%	70.06%	58.08%	-

of the probabilistic kinematic analysis reveal the potential types of failure that can occur and their relation from a risk perspective. The probabilistic empirical rock mass classifications show the conditional probability of each rock mass class or the confidence interval (*CI*) of the output. Different failure criteria and scenarios lead to various outcomes in limit equilibrium and numerical modelling. Incorporating the joint network into the model using the jointed GHB criterion results in a decreased Factor of Safety (*FoS*) and an increased Probability of Failure (*PoF*) compared to the homogenous GHB. The type of failure also differs in these analyses. These differences are known as modelling uncertainty resulting from the mathematical-mechanical process during modelling.

This paper has made numerous contributions to rock engineering studies, including (i) Defining the difference between civil and mining engineering projects regarding rock slope design and development requirements. (ii) Developing comprehensive flowcharts for probabilistic analysis in four different methods. (iii) Introducing the probabilistic Q_{slope} method for empirical rock mass classification approach and probabilistic kinematic analysis to determine the probability of occurring for wedge (P_{oW}), planar (P_{oP}), and toppling (P_{oT}) failures as well as the total probability of occurring (P_{tK}). (iv) The sensitivity analysis between input and output values in probabilistic limit equilibrium is plotted and analysed, as well as the influence of different earthquake scenarios on the *PoF*. (v) Comparing probabilistic limit equilibrium and numerical modelling in different failure criteria and scenarios. (vi) and introducing the total *PoF* by combining probabilities from limit equilibrium (LE), numerical modelling, and kinematic analyses in various scenarios. As for future research, this study suggests employing the slope stochastic seismic dynamic analysis in rock slope stability for active tectonic countries. Another step from the total probability result is exploring risk analysis for rock slope failure as a potential avenue.

Abbreviations

FoS	Factor of Safety
LE	Limit Equilibrium
PoF	Probability of Failure
RMR	Rock Mass Rating
GSI	Geological Strength Index
SMR	Slope Mass Rating
DRMR	Directional rock mass rating
RMS	Rock Mass Strength
SSAM	Slope Stability Assessment Methodology
RQD	Rock Quality Designation
NSMR	New Slope Mass Rating
MCS	Monte Carlo Simulation
MC	Mohr-Coulomb
JRC	Joint Roughness Coefficient
JCS	Joint Compressive Strength
HB	Hoek-Brown
BB	Barton-Bandis
FEM	Finite Element Method
FDM	Finite Difference Method
BEM	Boundary Element Method
DEM	Distinct Element Method
SRM	Shear Strength Reduction
P_{tK}	Total Probability of Occurrence
SRS	Simple Random Sampling
LHS	Latin Hypercube Sampling
PEM	Point Estimate Method
CI	Confidence Intervals or Credible Intervals
HDI	High-Density Interval
RMC	Rock Mass Classifications
PDF	probability density function
RI	Reliability Index
CR	Coefficient of Reliability
GSF	Great Sumatra Fault
SRF	Stress/Strength Reduction Factor
UCS	Uniaxial Compressive Strength
Mw	moment magnitude
PGA	peak ground acceleration
SRM	Strength Reduction Method
GHB	Generalised Hoek Brown
BBD	Box-Behnken Design
MCMC	Markov Chain Monte Carlo
FORM	First-Order Reliability Method
SORM	Second-Order Reliability Method
RS-DEM	Random Set District Element Method

QRA	Quantitative Risk Assessment
LSTM	long short-term memory
SVM	support vector machine
RF	random forest
CNN	convolutional neural network

Acknowledgements
The authors express their deepest gratitude to colleagues and students at the Department of Geological Engineering and Mining Engineering, Syiah Kuala University, for their support during fieldwork.

Author contributions
IR contributed to literature search, review, data analysis and writing-original draft preparation. IC and CZ contributed to the manuscript outline, conceptualisation, review, and editing. CW contributed to reviewing and editing. AM provided the idea and the data. All authors read and approved the final manuscript.

Funding
The authors are highly thankful to the Indonesia Endowment Fund for Education (LPDP), Ministry of Finance of the Republic of Indonesia, for providing the scholarship and research funding in 2022.

Data availability
The datasets used and/or analysed during the current study are available from the corresponding author on reasonable request.

Declarations

Competing interests
The authors declare no competing interests.

Received: 18 January 2024 / Accepted: 28 August 2024
Published online: 27 September 2024

References

Abdulai M, Sharifzadeh M (2019) Uncertainty and reliability analysis of open pit Rock slopes: a critical review of methods of analysis. Geotech Geol Eng 37(3):1223–1247. https://doi.org/10.1007/s10706-018-0680-y
Abdulai M, Sharifzadeh M (2021) Probability methods for Stability design of open pit Rock slopes: an overview. Geosciences 11(8):319–319. https://doi.org/10.3390/geosciences11080319
Adhari MR, Hidayat R (2023) A geological overview of the limestone members of the Woyla Group of Sumatra, Indonesia. J Geoscience Eng Environ Technol 8(3):189–195
Ahmadabadi M, Poisel R (2016) Probabilistic analysis of Rock Slopes Involving correlated non-normal variables using Point Estimate methods. Rock Mech Rock Eng 49(3):909–925. https://doi.org/10.1007/s00603-015-0790-2
Aladejare AE, Akeju VO (2020) Design and sensitivity analysis of Rock Slope using Monte Carlo Simulation. Geotech Geol Eng 38(1):573–585. https://doi.org/10.1007/s10706-019-01048-z
Aladejare AE, Wang Y (2018) Influence of rock property correlation on reliability analysis of rock slope stability: from property characterization to reliability analysis. Geosci Front 9(6):1639–1648. https://doi.org/10.1016/j.gsf.2017.10.003
Asem P, Gardoni P (2021) A generalized bayesian approach for prediction of strength and elastic properties of rock. Eng Geol 289. https://doi.org/10.1016/j.enggeo.2021.106187
Azarafza M, Koçkar MK, Zhu HH (2022) Correlations of SMR-Qslope Data in Stability classification of Discontinuous Rock Slope: a modified relationship considering the Iranian Data. Geotech Geol Eng 40(4):1751–1764. https://doi.org/10.1007/s10706-021-01991-w
Baecher GB, Christian JT (2005) Reliability and statistics in geotechnical engineering. Wiley
Bar N, Barton N (2017) The Q-Slope method for Rock Slope Engineering. Rock Mech Rock Eng 50(12):3307–3322. https://doi.org/10.1007/s00603-017-1305-0
Barber AJ (2000) The origin of the Woyla terranes in Sumatra and the late mesozoic evolution of the Sundaland margin. J Asian Earth Sci 18(6):713–738. https://doi.org/10.1016/S1367-9120(00)00024-9
Barber AJ, Crow MJ (2005) Pre-tertiary stratigraphy Sumatra: Geology, resources and Tectonic Evolution, vol 31. Geological Society, of London, pp 0–0
Barton N (1973) Review of a new shear-strength criterion for rock joints. Eng Geol 7(4):287–332. https://doi.org/10.1016/0013-7952(73)90013-6
Barton N (2013) Shear strength criteria for rock, rock joints, rockfill and rock masses: problems and some solutions. J Rock Mech Geotech Eng 5(4):249–261. https://doi.org/10.1016/j.jrmge.2013.05.008
Barton N, Bandis S (1982) Effects of block size on the shear behavior of jointed rock. In: The 23rd US symposium on rock mechanics (USRMS), OnePetro
Barton N, Pandey SK (2011) Numerical modelling of two stoping methods in two Indian mines using degradation of c and mobilization of φ based on Q-parameters. Int J Rock Mech Min Sci 48(7):1095–1112. https://doi.org/10.1016/j.ijrmms.2011.07.002
Barton N, Lien R, Lunde J (1974) Engineering Classification of Rock Masses for the Design of Tunnel Support Rock Mechanics. vol 6, p 13–13
Basahel H, Mitri H (2019) Probabilistic assessment of rock slopes stability using the response surface approach – a case study. Int J Min Sci Technol 29(3):357–370. https://doi.org/10.1016/j.ijmst.2018.11.002
Bedi A (2013) A proposed framework for characterising uncertainty and variability in rock mechanics and rock engineering
Begg SH, Welsh MB, Bratvold RB (2014) Uncertainty vs. variability: What's the difference and why is it important? SPE Hydrocarbon Economics and Evaluation Symposium(October):273–293 https://doi.org/10.2118/169850-ms
Bieniawski ZT (1989) Engineering rock mass classifications: a complete manual for engineers and geologists in mining, civil, and petroleum engineering. Wiley
Bray JD, Travasarou T (2009) Pseudostatic coefficient for use in simplified seismic slope stability evaluation. J Geotech GeoEnviron Eng 135(9):1336–1340
Brideau MA, Chauvin S, Andrieux P, Stead D (2012) Influence of 3D statistical discontinuity variability on slope stability conditions. Lateral 90(000)
Budetta P (2020) Some remarks on the use of deterministic and probabilistic approaches in the evaluation of rock slope stability. Geosci (Switzerland) 10(5). https://doi.org/10.3390/geosciences10050163
Cai M (2011) Rock mass characterization and rock property variability considerations for tunnel and cavern design. Rock Mech Rock Eng 44(4):379–399. https://doi.org/10.1007/s00603-011-0138-5
Celada B, Tardáguila I, Varona P, Rodríguez A, Bieniawski ZT (2014) Innovating Tunnel Design by an Improved Experience-based RMR System. In: The World Tunnel Congress 2014 – Tunnels for a better Life. 3: 1–9
Contreras LF, Brown ET, Ruest M (2018) Bayesian data analysis to quantify the uncertainty of intact rock strength. J Rock Mech Geotech Eng 10(1):11–31. https://doi.org/10.1016/j.jrmge.2017.07.008
Delignette-Muller ML, Dutang C (2015) Fitdistrplus: an R package for fitting distributions. J Stat Softw 64:1–34
Feng Y, Bozorgzadeh N, Harrison JP (2020) Bayesian analysis for uncertainty quantification of in situ stress data. Int J Rock Mech Min Sci 134(August):104381–104381. https://doi.org/10.1016/j.ijrmms.2020.104381
Hammah RE, Yacoub T, Corkum B, Curran JH (2008) The practical modelling of discontinuous rock masses with finite element analysis. In: The 42nd US Rock Mechanics Symposium (USRMS), OnePetro
Hammah RE, Yacoub TE, Curran JH (2009) Probabilistic slope analysis with the finite element method. In: 43rd US Rock Mechanics Symposium & 4th US-Canada Rock Mechanics Symposium, OnePetro
Hoek E, Brown ET (1997) Practical estimates of rock mass strength. Int J Rock Mech Min Sci 34(8):1165–1186. https://doi.org/10.1016/S1365-1609(97)80069-X
Hsu S-C, Nelson PP (2006) Material spatial variability and Slope Stability for weak Rock masses. J Geotech GeoEnviron Eng 132(2):183–193. https://doi.org/10.1061/(asce)1090-0241(2006)132:2(183)
Hu H, Huang Y, Zhao L, Xiong M (2022) Shaking table tests on slope reinforced by anchored piles under random earthquake ground motions. Acta Geotech 17(9):4113–4130
Huang Y, Xiong M (2017) Dynamic reliability analysis of slopes based on the probability density evolution method. Soil Dyn Earthq Eng 94:1–6
Huang Y, Xiong M, Zhao L (2022a) Numerical Simulation and Application of Slope Stochastic Seismic Response Analysis Slope Stochastic Dynamics. Springer, pp 53–83
Huang Y, Xiong M, Zhao L (2022b) Slope stochastic dynamics. Springer
Huang F, Xiong H, Chen S et al (2023) Slope stability prediction based on a long short-term memory neural network: comparisons with convolutional neural

networks, support vector machines and random forest models. Int J Coal Sci Technol 10(1):18
Hussain S, Rehman ZU, Khan NM et al (2021) Proposing a Viable Stabilization Method for Slope in a weak Rock Mass Environment using Numerical Modelling: a Case Study from Cut Slopes. J Min Environ 12(4):929–940
Hussin H, Arifin MH, Rusydy I, Lai GT, Udin WS (2024) Assessment of rock mass quality and rockfall potential evaluation for reclamation of a quarry. ASEAN Eng J 14(1):63–70. https://doi.org/10.11113/aej.V14.19950
Irsyam M, Cummins PR, Asrurifak M et al (2020) Development of the 2017 national seismic hazard maps of Indonesia. Earthq Spectra 36(1suppl):112–136. https://doi.org/10.1177/8755293020951206
Ito T, Gunawan E, Kimata F et al (2012) Isolating along-strike variations in the depth extent of shallow creep and fault locking on the northern Great Sumatran Fault. J Geophys Research: Solid Earth 117(6). https://doi.org/10.1029/2011JB008940
Keneti A, Pouragha M, Sainsbury BA (2021) Review of design parameters for discontinuous numerical modelling of excavations in the Hawkesbury Sandstone. Eng Geol 288. https://doi.org/10.1016/j.enggeo.2021.106158
Li Y, Tang C, Li D, Wu C (2020) A New Shear Strength Criterion of three-dimensional rock joints. Rock Mech Rock Eng 53(3):1477–1483. https://doi.org/10.1007/s00603-019-01976-5
Lu H, Kim E, Gutierrez M (2019) Monte Carlo simulation (MCS)-based uncertainty analysis of rock mass quality Q in underground construction. Tunn Undergr Space Technol 94(August):103089–103089. https://doi.org/10.1016/j.tust.2019.103089
Lu H, Kim E, Gutierrez M (2022) A probabilistic Q-system using the Markov chain to predict rock mass quality in tunneling. Comput Geotech 145(January). https://doi.org/10.1016/j.compgeo.2022.104689
Maazallahi V, Majdi A (2021) Directional rock mass rating (DRMR) for anisotropic rock mass characterization. Bull Eng Geol Environ 80:4471–4499. https://doi.org/10.1007/s10064-021-02143-3/Published
McQuillan A, Canbulat I, Payne D, Oh J (2018) New risk assessment methodology for coal mine excavated slopes. Int J Min Sci Technol 28(4):583–592. https://doi.org/10.1016/j.ijmst.2018.07.001
McQuillan A, Canbulat I, Oh J (2020) Methods applied in Australian industry to evaluate coal mine slope stability. Int J Min Sci Technol 30(2):151–155. https://doi.org/10.1016/j.ijmst.2019.11.001
Millard SP (2013) EnvStats: an R package for environmental statistics. Springer Science & Business Media
Obregon C, Mitri H (2019) Probabilistic approach for open pit bench slope stability analysis – a mine case study. Int J Min Sci Technol 29(4):629–640. https://doi.org/10.1016/j.ijmst.2019.06.017
Pantelidis L (2009) Rock slope stability assessment through rock mass classification systems. Int J Rock Mech Min Sci 46(2):315–325. https://doi.org/10.1016/j.ijrmms.2008.06.003
Park H, West TR (2001) Development of a probabilistic approach for rock wedge failure. Eng Geol 59(3):233–251. https://doi.org/10.1016/S0013-7952(00)00076-4
Park HJ, Um JG, Woo I, Kim JW (2012) The evaluation of the probability of rock wedge failure using the point estimate method. Environ Earth Sci 65(1):353–361. https://doi.org/10.1007/s12665-011-1096-7
Park H-J, Lee J-H, Kim K-M, Um J-G (2016) Assessment of rock slope stability using GIS-based probabilistic kinematic analysis. Eng Geol 203:56–69. https://doi.org/10.1016/j.enggeo.2015.08.021
Patton FD (1966) Multiple modes of shear failure in rock. 1st ISRM Congress. OnePetro
Pereira JP (1997) Rolling friction and shear behaviour of rock discontinuities filled with sand. J Rock Mech Mm Sci 34(4)
Priest SD, Hudson JA (1976) Discontinuity Spacings in Rock* Int J Rock Mech Min Sci & Geomech Abstr. vol 13. Pergamon Press, p 135–148
Revelle W, Revelle MW (2015) Package 'psych'. Compr R Archive Netw 337(338)
Romana M (1985) New adjustment ratings for application of Bieniawski classification to slopes. In: Proceedings of the international symposium on role of rock mechanics, Zacatecas, Mexico, p 49–53
Rosenbaum MS, Rosén L, Gustafson G (1997) Probabilistic models for estimating lithology. Eng Geol 47(1):43–55. https://doi.org/10.1016/S0013-7952(96)00118-4
Rosenblueth E (1981) Two-point estimates in probabilities. Appl Math Model 5(5):329–335. https://doi.org/10.1016/S0307-904X(81)80054-6
Rusydy I, Al-Huda N (2021) New rock mass classifications for limestone of the Woyla group and its empirical relationship in Aceh Province, Indonesia. Carbonates Evaporites 36(1). https://doi.org/10.1007/s13146-021-00677-x
Rusydy I, Faustino-Eslava DV, Muksin U et al (2017) Building vulnerability and human loss assessment in different earthquake intensity and time: A case study of the University of the Philippines, Los Baños (UPLB) Campus. In: IOP Conference Series: Earth and Environmental Science, vol 56
Rusydy I, Faustino-Eslava DV, Muksin U et al (2018a) GIS-based earthquake damage prediction in different earthquake models: a case study at the university of the Philippines Los Baños, Philippines. Philippine J Sci 147(2):301–316
Rusydy I, Muksin U, Mulkal, Idris Y, Akram MN (2018b) Syamsidik The prediction of building damages and casualties in the Kuta Alam sub district-Banda Aceh caused by different earthquake models. AIP Conference Proceedings 1987 https://doi.org/10.1063/1.5047297
Rusydy I, Al-Huda N, Fahmi M, Effendi N (2019) Kinematic analysis and rock mass classifications for rock slope failure at USAID highways. SDHM Struct Durab Health Monit 13(4):379–398. https://doi.org/10.32604/sdhm.2019.08192
Rusydy I, Al-huda N, Fahmi M, Effendi N, Muslim A, Lubis M (2020a) Analisis Modulus Deformasi Massa Batuan pada Segmen Jalan USAID km 27 hingga km 30 Berdasarkan Klasifikasi Massa Batuan. 30(1):93–106. https://doi.org/10.14203/risetgeotam2020.v30.1073
Rusydy I, Idris Y, Mulkal et al (2020b) Shallow crustal earthquake models, damage, and loss predictions in Banda Aceh, Indonesia. Geoenvironmental Disasters 7(1). https://doi.org/10.1186/s40677-020-0145-5
Rusydy I, Fathani TF, Al-Huda N et al (2021) Integrated approach in studying rock and soil slope stability in a tropical and active tectonic country. Environ Earth Sci 80(2):1–20. https://doi.org/10.1007/s12665-020-09357-w
Rusydy I, Mulkal M, Baramsyah H et al (2022) Rock slope kinematic analysis for planar failure: A probabilistic approach. In: E3S Web of Conferences,. vol 340. p 01017–01017
Sari M (2019) Stability analysis of cut slopes using empirical, kinematical, numerical and limit equilibrium methods: case of old Jeddah–Mecca road (Saudi Arabia). Environ Earth Sci 78(21). https://doi.org/10.1007/s12665-019-8573-9
Sari M, Karpuz C, Ayday C (2010) Estimating rock mass properties using Monte Carlo simulation: Ankara andesites. Comput Geosci 36(7):959–969. https://doi.org/10.1016/j.cageo.2010.02.001
Savely JP (1987) Probabilistic analysis of intensely fractured rock masses. 6th ISRM Congress. OnePetro
Selby MJ (1982) Controls on the stability and inclinations of hillslopes formed on hard rock. Earth Surf Proc Land 7(5):449–467
Shen H (2012) Non-deterministic analysis of slope stability based on numerical simulation. Freiberg
Singh RP, Dubey CS, Singh SK et al (2013) A new slope mass rating in mountainous terrain, Jammu and Kashmir Himalayas: application of geophysical technique in slope stability studies. Landslides 10(3):255–265. https://doi.org/10.1007/s10346-012-0323-y
Singh SK, Raval S, Banerjee BP (2021) Automated structural discontinuity mapping in a rock face occluded by vegetation using mobile laser scanning. Eng Geol 285:106040
Stead D, Wolter A (2015) A critical review of rock slope failure mechanisms: The importance of structural geology Journal of Structural Geology. vol 74. Elsevier, p 1–23
Stead D, Eberhardt E, Coggan JS (2006) Developments in the characterization of complex rock slope deformation and failure using numerical modelling techniques. Eng Geol 83(1–3):217–235. https://doi.org/10.1016/j.enggeo.2005.06.033
Wajzer MR, Barber AJ, Hidayat S, Suharsono (1991) Accretion, collision and strike-slip faulting: the Woyla group as a key to the tectonic evolution of North Sumatra. J Southeast Asian Earth Sci 6(3):447–461. https://doi.org/10.1016/0743-9547(91)90087-E
Walpole RE, Myers RH, Myers SL, Ye K (2011) Probability and Statistics for Engineers and Scientists, 9th edn. Pearson
Wyllie DC (2018) Rock Slope Engineering: Civil Applications, Fifth Edition, Fifth Edition edn. CRC Press, Boca Raton
Wyllie DC, Mah C (2004) Rock slope engineering: Civil and Mining, 4Th Edition edn. Spon Press, London
Yan J, Chen J, Li Y et al (2022) Kinematic-based failure angle analysis for discontinuity-controlled rock slope instabilities: a case study of Ren Yi Peak Cluster in Fusong County, China. Nat Hazards 111(3):2281–2296. https://doi.org/10.1007/s11069-021-05137-2
Yang G, Chen Y, Liu X, Yang R, Zhang Y, Zhang J (2023) Stability analysis of a slope containing water-sensitive mudstone considering different rainfall conditions at an open-pit mine. Int J Coal Sci Technol 10(1):64

Zhang C, Mitra R, Hebblewhite B (2012) Review of numerical modelling evaluation of mechanisms for valley closure subsidence under irregular topographic condition. In: ISRM International Symposium-EUROCK 2012,. OnePetro

Zhang Q, Huang X, Zhu H, Li J (2019) Quantitative assessments of the correlations between rock mass rating (RMR) and geological strength index (GSI). Tunn Undergr Space Technol 83:73–81. https://doi.org/10.1016/j.tust.2018.09.015

Zhang Wg M, Fs C, Fy L Hl (2021) Effects of spatial variability of weak layer and seismic randomness on rock slope stability and reliability analysis. Soil Dyn Earthq Eng 146(March 2020):106735–106735. https://doi.org/10.1016/j.soildyn.2021.106735

Zhao LH, Zuo S, Li L, Lin Y, Zhang YB (2016) System reliability analysis of plane slide rock slope using Barton-Bandis failure criterion. Int J Rock Mech Min Sci 88:1–11. https://doi.org/10.1016/j.ijrmms.2016.06.003

Zhao Y, He X, Jiang L, Wang Z, Ning J, Sainoki A (2023) Influence analysis of complex crack geometric parameters on mechanical properties of soft rock. Int J Coal Sci Technol 10(1):78

Zheng J, Zhao Y, Lü Q, Deng J, Pan X, Li Y (2016) A discussion on the adjustment parameters of the Slope Mass Rating (SMR) system for rock slopes. Eng Geol 206:42–49. https://doi.org/10.1016/j.enggeo.2016.03.007

Zhou X, Chen J, Chen Y, Song S (2017) Bayesian-based probabilistic kinematic analysis of discontinuity-controlled rock slope instabilities. Bull Eng Geol Environ 76(4):1249–1262. https://doi.org/10.1007/s10064-016-0972-5

Zienkiewicz OC, Humpheson C, Lewis RW (1975) Associated and non-associated visco-plasticity and plasticity in soil mechanics. Geotechnique 25(4):671–689

Publisher's note